

# Ultra-Directional Transition Radiation From Deep-Subwavelength Epsilon-Near-Zero Metamaterials

Zun Wang, Zheng Gong, Ruoxi Chen, Xiangfeng Xi, Jialin Chen, Yi Yang,  
 Hongsheng Chen,\* Erping Li, Ido Kaminer,\* and Xiao Lin\*

Transition radiation occurs whenever free electrons penetrate an optical sample and offers a powerful route to create light emission for arbitrary frequencies, which is crucial to numerous interdisciplinary applications. However, this type of light emission generally has a broad angular distribution and weak intensity, especially when the sample thickness is subwavelength. Accordingly, ultra-thick samples are required in practical applications and fundamentally inhibit enticing on-chip applications. Here, a mechanism is theoretically revealed to create ultra-directional transition radiation with enhanced intensity from epsilon-near-zero metamaterials with a deep-subwavelength thickness, down to one hundredth of the light wavelength. The underlying mechanism lies in the extreme photonic density of states that can couple to free space within a predefined angular range through the judicious design of metamaterials' anisotropy. Specifically, by tailoring one component of metamaterials' relative permittivity to be near zero and the other much larger than unity, the radiation peak can exhibit a narrow angular spread with full width at half maximum much smaller than one degree, along with a three-order-of-magnitude enhancement in intensity. Moreover, this ultra-high directionality is robust to variations in electron velocity and can be achieved by low-energy electrons. The finding may pave the way toward the development of novel on-chip photonic devices.

It could happen whenever the charged particles (e.g., free electrons) pass through inhomogeneous media, such as an optical interface separating different media. As further predicted by Garibian in 1959,[2] the intensity of X-ray transition radiation increases linearly with the Lorentz factor  $\gamma = 1/\sqrt{1 - v^2/c^2}$ , when the particle velocity  $v$  approaches the speed of light  $c$  in vacuum. This unique feature enables the wide use of transition radiation in high-energy physics and astrophysics,[7–10] especially for the beam diagnosis and the identification of particles with extremely high energies (e.g., those with a kinetic energy larger than 100 giga-electron-volts or  $\gamma > 10^5$ ). On the other hand, while the transition radiation is capable to create light emission at any frequency regime,[11–13] ranging from microwave to X-ray, the generation of transition radiation itself does not have any fundamental requirement on the particle velocity. In stark contrast, Cherenkov radiation[14–20] always requires the particle velocity to exceed the Cherenkov threshold (i.e., the phase velocity of light

in the host medium),[21–24] by which all practical applications of Cherenkov radiation[25–30] are limited. Compared to the Cherenkov radiation, the transition radiation provides an indispensable and complementary route for the development of

## 1. Introduction

Transition radiation,[1–6] as theoretically proposed by Ginzburg and Frank in 1946, is a typical type of free-electron radiation.

Z. Wang  
 Chu Kochen Honors College  
 Zhejiang University  
 Hangzhou 310012, China

Z. Gong, R. Chen, X. Xi, H. Chen, E. Li, X. Lin  
 Interdisciplinary Center for Quantum Information  
 State Key Laboratory of Extreme Photonics and Instrumentation  
 Zhejiang Key Laboratory of Intelligent Electromagnetic Control and Advanced Electronic Integration  
 College of Information Science & Electronic Engineering  
 Zhejiang University  
 Hangzhou 310027, China  
 E-mail: [hansomchen@zju.edu.cn](mailto:hansomchen@zju.edu.cn); [xiaolinzju@zju.edu.cn](mailto:xiaolinzju@zju.edu.cn)

Z. Gong, R. Chen, X. Xi, H. Chen, E. Li, X. Lin  
 International Joint Innovation Center  
 The Electromagnetics Academy at Zhejiang University  
 Zhejiang University  
 Haining 314400, China

J. Chen  
 State Key Laboratory of Space-Ground Integrated Information Technology  
 Beijing Institute of Satellite Information Engineering  
 Beijing 100095, China

Y. Yang  
 Department of Physics  
 University of Hong Kong  
 Hong Kong 999077, China

I. Kaminer  
 Department of Electrical and Computer Engineering  
 Technion-Israel Institute of Technology  
 Haifa 32000, Israel  
 E-mail: [kaminer@technion.ac.il](mailto:kaminer@technion.ac.il)

 The ORCID identification number(s) for the author(s) of this article can be found under <https://doi.org/10.1002/adom.202501449>

DOI: 10.1002/adom.202501449

integrated light sources at previously hard-to-reach frequency regimes (e.g., terahertz, ultraviolet, and X-ray) readily by exploiting low-energy particles.<sup>[24,31,32]</sup> Because of these enticing features, transition radiation is crucial to many interdisciplinary applications, ranging from particle detectors,<sup>[33,34]</sup> compact light sources,<sup>[35–39]</sup> nanophotonics,<sup>[40–43]</sup> plasmonics,<sup>[44–48]</sup> material science<sup>[49–54]</sup> to bio-imaging.<sup>[55,56]</sup>

However, the transition radiation typically suffers from poor directionality and low intensity. These intrinsic drawbacks fundamentally impede the further development of many promising transition-radiation-based applications, especially for those on chips.<sup>[57–59]</sup> While the enhancement of the intensity of transition radiation has been widely investigated and could be achieved,<sup>[11,60,61]</sup> for example, via the usage of high-current electron beams, there is comparatively less research on how to improve the directionality of transition radiation.

Currently, the improvement of the directionality of transition radiation primarily relies on two conventional approaches. The first approach is to use high-energy particles<sup>[12]</sup> (e.g., those with  $\gamma > 100$  or the kinetic energy larger than 500 MeV). Under this scenario, there is always the emergence of a sharp radiation peak at the angle  $\theta_p$ , which is closely related to the Lorentz factor  $\gamma$ ,<sup>[1,2]</sup> namely  $\theta_p = 1/\gamma$ . Generally, a larger kinetic energy of particles could lead to a better directionality of transition radiation. The second approach is to increase the interaction length between the charged particle and the designed sample. As a typical example, the coherent X-ray transition radiation with a sharp angular peak could be created using multilayer conducting foil plates, whose thickness spans several meters.<sup>[7]</sup> Similarly, the resonance transition radiation with high directionality can be achieved via photonic crystals,<sup>[8,21,24,62]</sup> whose total thickness is generally two orders of magnitude larger than the working wavelength of light. By following this thought, Ref. [63] further showed that the so-called pseudo-Brewster effect of gain media could give rise to the exotic phenomenon of Brewster-transition radiation, whose ultra-high directionality always shows up at the Brewster angle, regardless of the particle velocity. Yet, the creation of this Brewster-transition radiation requires the thickness of the gain slabs to be one order of magnitude larger than the working wavelength of light.

For these conventional approaches, generating high-energy particles requires a complex yet giant acceleration infrastructure, which is not favorable for designing compact light sources. Meanwhile, the low-energy particles cannot safely penetrate through these thick samples, mainly due to the potential occurrence of inelastic particle scattering. To mitigate this issue, a hole with its center along the particle trajectory should be drilled inside these thick samples.<sup>[57]</sup> Despite this scheme being in principle feasible, it would tremendously increase the complexity during the sample fabrication and the measurement of light emission. This way, to facilitate the development of integrated free-electron radiation sources, it is highly wanted to create the transition radiation simultaneously with enhanced intensity and improved directionality from thin samples (e.g., those with a subwavelength thickness<sup>[64,65]</sup>), especially by exploiting low-energy particles. Despite extensive research on free-electron radiation,<sup>[66–75]</sup> this goal remains a long-standing open challenge that is highly sought after.

Here, we find a route to achieve the ultra-directional transition radiation with enhanced intensity by exploiting deep-

subwavelength anisotropic epsilon-near-zero metamaterials. To be specific, the relative permittivity of anisotropic metamaterials should have one component close to zero, but the other components much larger than unity. Under this scenario, the emerging radiation peak could have its angular spread much smaller than one degree, along with its intensity enhanced by three orders of magnitude, even when the thickness of anisotropic epsilon-near-zero metamaterials is down to one hundredth of the working wavelength of light. To place our theoretical findings in the proper context, the exploration of the transition radiation from epsilon-near-zero media is traced back to the pioneering work of Ferrell in 1958.<sup>[76]</sup> While the epsilon-near-zero media<sup>[77–82]</sup> (e.g., isotropic metals and uniaxial boron nitrides) are widely known to be capable of enhancing the intensity of transition radiation,<sup>[47,83–87]</sup> the possibility to further improve the directionality of transition radiation from subwavelength epsilon-near-zero media remains elusive. Our finding further indicates that the judicious design of the anisotropy of epsilon-near-zero metamaterials could offer an extra degree of freedom to simultaneously engineer the directionality and intensity of transition radiation on demand. This way, the anisotropic epsilon-near-zero metamaterials are promising to provide a versatile platform for the flexible manipulation of particle-matter interactions and for the development of novel integrated photonic devices based on free-electron radiation, such as compact light sources and particle detectors.

## 2. Result

We begin with the conceptual demonstration of the ultra-directional transition radiation with enhanced intensity from a subwavelength anisotropic epsilon-near-zero metamaterial slab in **Figure 1**. The anisotropic epsilon-near-zero metamaterial has a thickness  $d$  and a positive relative permittivity  $\bar{\epsilon}_r = [\epsilon_{\perp}, \epsilon_{\perp}, \epsilon_z]$  in **Figure 1a**, such as  $d/\lambda_0 = 0.1$ ,  $\epsilon_z = 0.1$ , and  $\epsilon_{\perp} = 70$  used in **Figure 1b–e** for conceptual illustrations. These desired anisotropic epsilon-near-zero metamaterials in principle, could be implemented by using the effective-medium approach (see Figures S3–S5, Supporting Information). For conceptual clarity, the electron velocity is set to be smaller than the Cherenkov threshold, namely  $v/c \leq \min(\frac{1}{\sqrt{\epsilon_{\perp}}}, \frac{1}{\sqrt{\epsilon_z}})$ , in order to eliminate the emergence of Cherenkov radiation.

By launching charged particles to bombard a subwavelength anisotropic epsilon-near-zero metamaterial slab, the total angular spectral energy density  $U(\theta)$  of emitted light at the working wavelength  $\lambda_0$  is analytically calculated by extending Ginzburg and Frank's theory of transition radiation.<sup>[1,2,8,24,87]</sup> The radiation angle  $\theta$  corresponds to the angle between  $\vec{k}$  and  $\vec{k}_z$ , where  $\vec{k} = \vec{k}_{\perp} + \vec{k}_z$  is the wavevector of emitted light inside the vacuum region and  $\vec{k}_z = \hat{z}\vec{k}_z$ . From **Figure 1b–d**, there is a strong and sharp radiation peak at the radiation angle  $\theta = \theta_p$ , namely  $\max(U(\theta)) = U(\theta_p)$ . Remarkably, the angular width  $\Delta\theta$  or the angular full width at half maximum of this radiation peak is less than one degree, namely  $\Delta\theta = 0.8^\circ$  in **Figure 1b,d**. Meanwhile, the intensity of this radiation peak from anisotropic metamaterials (e.g.,  $\epsilon_z = 0.1$  and  $\epsilon_{\perp} = 70$  in **Figure 1d**) could be three orders of magnitude larger than that from isotropic materials (e.g.,  $\epsilon_z = \epsilon_{\perp} = 5$  in **Figure 1c**) with the same slab thickness.

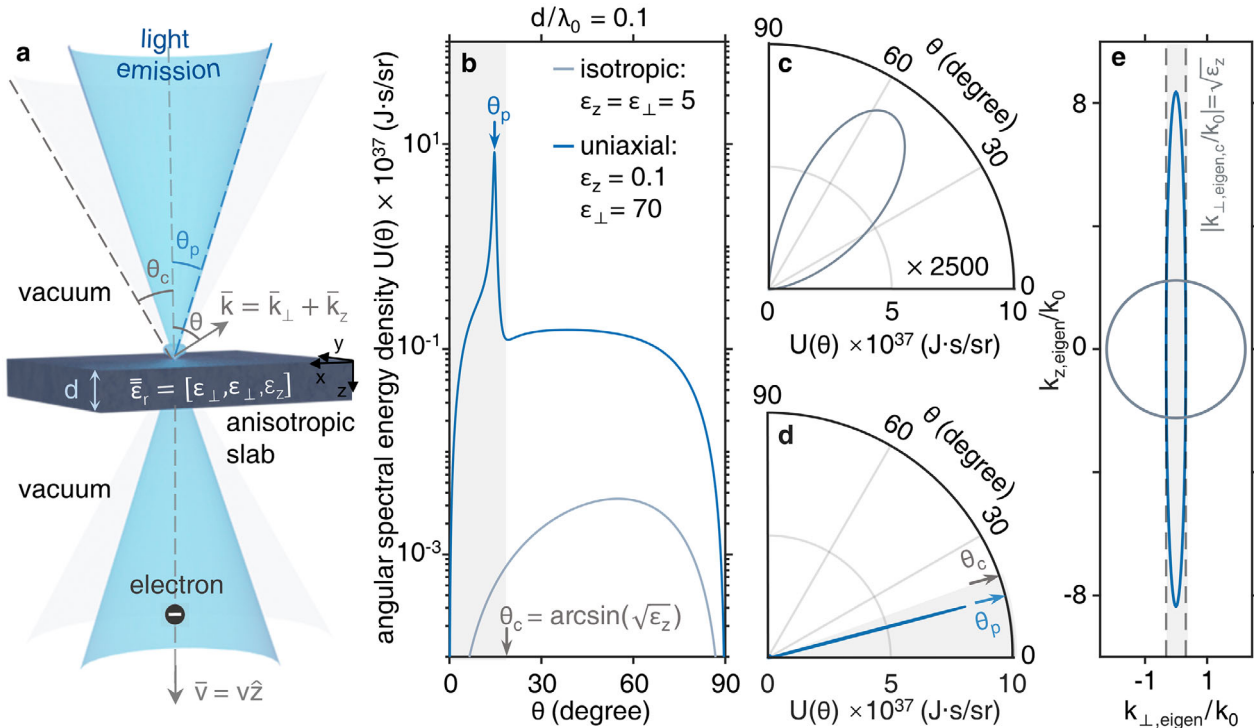


**Figure 1.** Conceptual demonstration of the ultra-directional transition radiation with enhanced intensity from a subwavelength anisotropic metamaterial slab. a) Structural schematic. The swift electron moves with a velocity of  $\bar{v} = \hat{z}\nu$ . The anisotropic metamaterial is surrounded by vacuum and has a thickness  $d$  and a relative permittivity  $\bar{\epsilon}_r = [\epsilon_\perp, \epsilon_\perp, \epsilon_z]$ . The emitted light in a vacuum has a wavevector  $\bar{k} = \bar{k}_\perp + \bar{k}_z$ , where  $\bar{k}_z = \hat{z}k_z$ . Accordingly, the radiation angle  $\theta$  in vacuum corresponds to the angle between  $\bar{k}$  and  $\bar{k}_z$ . Without further specification, here and below, we set  $\nu/c = 0.1$ ,  $d/\lambda_0 = 0.1$ ,  $\epsilon_z = 0.1$ , and  $\epsilon_\perp = 70$ , where  $c$  is the speed of light in vacuum, and  $\lambda_0$  (e.g.,  $\lambda_0 = 12.2 \mu\text{m}$ ) is the working wavelength of light in vacuum. b-d) Angular spectral energy density  $U(\theta)$  of emitted light in Cartesian or polar coordinates. A strong and sharp radiation peak shows up at  $\theta = \theta_p$ .  $\theta_c = \arcsin(\sqrt{\epsilon_z})$  is the critical angle of incidence, above which the photonic modes in the metamaterial would be totally reflected and could not couple into free space. e) Isofrequency contours of propagating eigenmodes inside anisotropic epsilon-near-zero metamaterials. These eigenmodes have a wavevector  $\bar{k}_{\text{eigen}} = \hat{1}k_{\perp,\text{eigen}} + \hat{2}k_{z,\text{eigen}}$ , where  $\frac{k_{\perp,\text{eigen}}^2}{\epsilon_z} + \frac{k_{z,\text{eigen}}^2}{\epsilon_\perp} = (\frac{2\pi}{\lambda_0})^2$ . For comparison, the case from an isotropic material (e.g.,  $\epsilon_z = \epsilon_\perp = 5$ ) is also shown in (b-e).

This revealed phenomenon of ultra-directional transition radiation with enhanced intensity in Figure 1b-d is fundamentally related to the isofrequency contour of propagating eigenmodes inside anisotropic epsilon-near-zero metamaterials. To be specific, their isofrequency contour is governed by  $\frac{k_{\perp,\text{eigen}}^2}{\epsilon_z} + \frac{k_{z,\text{eigen}}^2}{\epsilon_\perp} = k_0^2$ , where  $\bar{k}_{\text{eigen}} = \hat{1}k_{\perp,\text{eigen}} + \hat{2}k_{z,\text{eigen}}$  is the wavevector of these eigenmodes inside the metamaterial and  $k_0 = \frac{2\pi}{\lambda_0}$ . When  $\epsilon_z \rightarrow 0^+$  and  $\epsilon_\perp > 0$ , the corresponding elliptical isofrequency contour in the  $k_{\perp,\text{eigen}} - k_{z,\text{eigen}}$  parameter space is located within a very narrow wavevector range, namely  $k_{\perp,\text{eigen}} \in [-k_{\perp,\text{eigen},c}, k_{\perp,\text{eigen},c}]$  in Figure 1e, where  $\lim_{\epsilon_z \rightarrow 0^+} k_{\perp,\text{eigen},c} = \lim_{\epsilon_z \rightarrow 0^+} \sqrt{\epsilon_z}k_0 \ll k_0$ . If  $\epsilon_z \rightarrow 0^+$  and  $\epsilon_\perp \gg 1$ , Figure 1e shows that the anisotropic epsilon-near-zero metamaterial could also support the propagation of high- $k$  (i.e., high-momentum) eigenmodes. In other words, these high- $k$  eigenmodes inside anisotropic epsilon-near-zero metamaterials could not only be excited by swift electrons but also be capable of transmitting into the vacuum region. According to the momentum-matching condition at the vacuum-metamaterial interface, we have  $\bar{k}_\perp = \bar{k}_{\perp,\text{eigen}}$  and thus  $|\bar{k}_\perp| \leq k_{\perp,\text{eigen},c}$ . That is, these excited eigenmodes only contribute to the emitted light within the angular range of  $\theta \in (0, \theta_c]$ , where

$\theta_c = \arcsin(k_{\perp,\text{eigen},c}/k_0) = \arcsin \sqrt{\epsilon_z}$  represents the critical angle of incidence, above which the total reflection would happen at the vacuum-metamaterial interface. Moreover, when  $\epsilon_z \rightarrow 0^+$  and  $\epsilon_\perp \gg 1$ , the elliptical isofrequency contour in Figure 1e is to some extent alike two parallel lines. This directly leads to most high- $k$  eigenmodes having value of  $|k_{\perp,\text{eigen}}|$  very close to  $k_{\perp,\text{eigen},c}$ . This further indicates the possibility that these excited eigenmodes with a large photonic density of states primarily contribute to the emitted light at an angle (i.e.,  $\theta_p$  in Figure 1b) close to  $\theta_c$ , such as  $\theta_p = 14.8^\circ$  and  $\theta_c = 18.4^\circ$  in Figure 1b. This is exactly the fundamental reason for the emergence of a strong and sharp peak at  $\theta = \theta_p$  in Figure 1b. As a result, the maximum intensity of emitted light with  $\theta \in (0^\circ, \theta_c]$  is generally much larger than that with  $\theta \in (\theta_c, 90^\circ)$ . For completeness, we show in Figure S6 (Supporting Information) that other types of epsilon-near-zero metamaterials (e.g.,  $\epsilon_\perp \rightarrow 0$ ) do not exhibit the unique isofrequency contours required for the emergence of ultra-directional transition radiation. For clarity, below we define the angular spectral factor as  $\eta = \max(U(\theta), \theta \leq \theta_c)/\max(U(\theta), \theta > \theta_c)$ . To be specific, we have  $\eta = 54$  in Figure 1b. That is, the peak intensity with  $\theta \in (0^\circ, \theta_c]$  is almost two orders of magnitude larger than that with  $\theta \in (\theta_c, 90^\circ)$ .

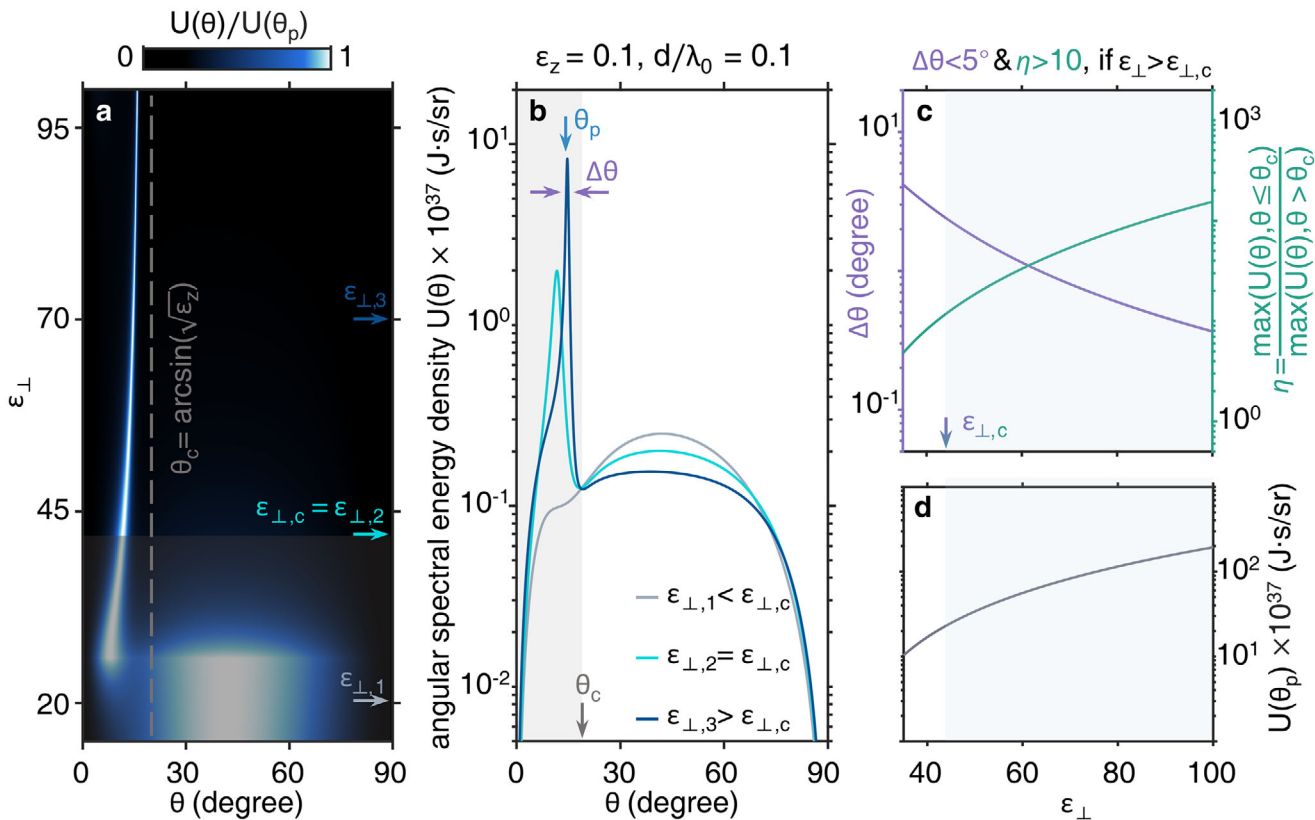


**Figure 2.** Influence of  $\epsilon_{\perp}$  on the ultra-directional transition radiation with enhanced intensity from subwavelength anisotropic metamaterial slabs. a) Normalized angular spectral energy density  $U(\theta)/U(\theta_p)$  of emitted light in the  $\theta - \epsilon_{\perp}$  parameter space. The angular width  $\Delta\theta$  corresponds to the full width at half maximum of the radiation peak at  $\theta = \theta_p$ . The angular spectral factor is mathematically defined as  $\eta = \max(U(\theta), \theta \leq \theta_c)/\max(U(\theta), \theta > \theta_c)$ .  $\epsilon_{\perp,c}$  corresponds to the critical value of  $\epsilon_{\perp}$ , above which we always have  $\Delta\theta \leq 5^\circ$  and  $\eta \geq 10$ , for example in (a),  $\epsilon_{\perp,c} = 42$ . b) Angular spectral energy density  $U(\theta)$  of emitted light for different values of  $\epsilon_{\perp}$ , such as  $\epsilon_{\perp,1} = 20 < \epsilon_{\perp,c}$ ,  $\epsilon_{\perp,2} = 42 = \epsilon_{\perp,c}$ , and  $\epsilon_{\perp,3} = 70 > \epsilon_{\perp,c}$  used in (b). c) Dependence of the angular width  $\Delta\theta$  and the angular spectral factor  $\eta$  on  $\epsilon_{\perp}$ . d) Dependence of the peak intensity  $U(\theta_p)$  on  $\epsilon_{\perp}$ . If  $\epsilon_{\perp}$  increases,  $\Delta\theta$  decreases and  $U(\theta_p)$  increases.

From the above analysis, both  $\epsilon_{\perp}$  and  $\epsilon_z$  play a crucial role in determining the elliptical isofrequency contour shape of propagating eigenmodes inside anisotropic metamaterials. This way, it is reasonable to expect that both  $\epsilon_{\perp}$  and  $\epsilon_z$  would significantly influence the performance of the revealed ultra-directional transition radiation with enhanced intensity, as shown in Figures 2–3.

We start with the investigation of the influence of  $\epsilon_{\perp}$  on the ultra-directional transition radiation with enhanced intensity in Figure 2. From Figure 2a,b, when  $\epsilon_{\perp}$  is larger than a critical value  $\epsilon_{\perp,c}$  (i.e.,  $\epsilon_{\perp} \geq \epsilon_{\perp,c} = 42$  in Figure 2a), we always have the angular width  $\Delta\theta \leq 5^\circ$  and the angular spectral factor  $\eta \geq 10$ . To facilitate the discussion, below we denote that the revealed phenomenon of ultra-directional transition radiation with enhanced intensity emerges only when both conditions of  $\Delta\theta \leq 5^\circ$  and  $\eta \geq 10$  are fulfilled. When  $\epsilon_{\perp}$  is larger than  $\epsilon_{\perp,c}$  and further increases, the radiation peak would become sharper and stronger, and the peak angle  $\theta_p$  would be much closer to the critical angle  $\theta_c = 18.4^\circ$  in Figure 2. To be specific, when  $\epsilon_{\perp}$  increases from 42 to 100, the angular width  $\Delta\theta$  decreases from  $5^\circ$  to  $0.3^\circ$  in Figure 2c, the angular spectral factor  $\eta$  increases from 10 to 150 in Figure 2c, and the peak angle  $\theta_p$  increases from  $11.6^\circ$  to  $15.9^\circ$  in Figure 2a. Moreover, the peak intensity  $U(\theta_p)$  at the case with  $\epsilon_{\perp} = 100$  is more than one order of magnitude larger than that at the case

with  $\epsilon_{\perp} = 42$  in Figure 2d. By contrast, when  $\epsilon_{\perp}$  is smaller than  $\epsilon_{\perp,c}$  and further decreases, the transition radiation would have worse directionality and weaker intensity. Particularly, when  $\epsilon_{\perp} \ll \epsilon_{\perp,c}$  (e.g.,  $\epsilon_{\perp} = 20$  in Figure 2a,b), the radiation peak begins to show up at the angle  $\theta_p = 42.1^\circ > \theta_c$  and has a large angular width of  $\Delta\theta = 48^\circ$ .

We investigate the influence of  $\epsilon_z$  on the ultra-directional transition radiation with enhanced intensity in Figure 3a,b. From Figure 3, the reduction of  $\epsilon_z$  (i.e., by letting  $\epsilon_z \rightarrow 0^+$ ) could also give rise to a sharper and stronger radiation peak. To be specific, when  $\epsilon_{\perp} = 70$  and  $\epsilon_z$  decreases from 0.2 to 0.01 in Figure 3a, the angular width  $\Delta\theta$  decreases from  $1.2^\circ$  to  $0.2^\circ$ , and the peak intensity of  $U(\theta_p)$  is enhanced by over one order of magnitude. On the other hand, since the critical angle is governed by  $\theta_c = \arcsin \sqrt{\epsilon_z}$ , the manipulation of  $\epsilon_z \rightarrow 0^+$  directly leads to the occurrence of radiation peak at a smaller angle (i.e.,  $\theta_p \rightarrow 0^\circ$ ), which is also much closer to the critical angle (i.e.,  $|\theta_c - \theta_p| \rightarrow 0^\circ$ ). For example, when  $\epsilon_z$  decreases from 0.2 to 0.01 in Figure 3a, the peak angle  $\theta_p$  decreases from  $21.0^\circ$  to  $4.6^\circ$ , and the value of  $|\theta_c - \theta_p|$  decreases from  $5.6^\circ$  to  $1.1^\circ$ .

We now proceed to discuss the influence of slab thickness  $d$  on the ultra-directional transition radiation with enhanced intensity in Figure 4. From Figure 4a, when the slab thickness decreases,

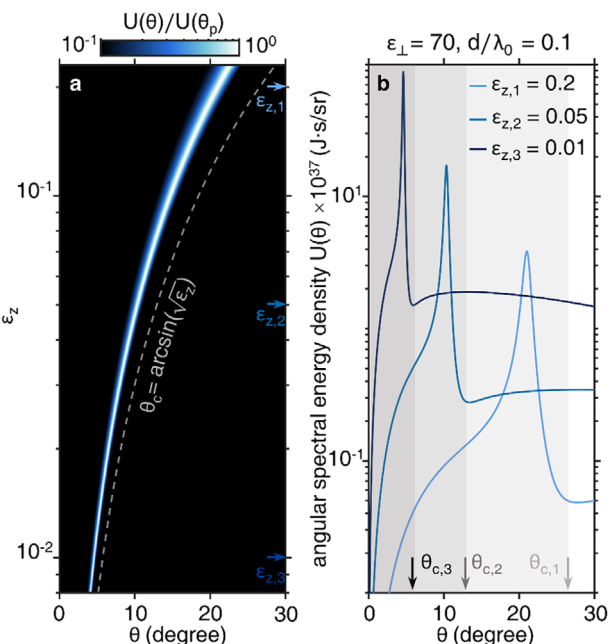


**Figure 3.** Influence of  $\epsilon_z$  on the ultra-directional transition radiation with enhanced intensity from subwavelength anisotropic metamaterial slabs. a) Normalized angular spectral energy density  $U(\theta)/U(\theta_p)$  of emitted light in the  $\theta - \epsilon_z$  parameter space. b) Angular spectral energy density  $U(\theta)$  of emitted light for different values of  $\epsilon_z$ . If  $\epsilon_z$  decreases to zero (i.e.,  $\epsilon_z \rightarrow 0^+$ ),  $\Delta\theta$  decreases and  $U(\theta_p)$  increases.

the phenomenon of ultra-directional transition radiation with enhanced intensity might disappear. In other words, the emergence of ultra-directional transition radiation with enhanced intensity (i.e.,  $\Delta\theta \leq 5^\circ$  and  $\eta \geq 10$ ) requires the slab thickness at least larger than a critical thickness  $d_c$ , namely  $d \geq d_c$ . For example, the critical slab thickness is down to  $d_c/\lambda_0 = 0.062$ , if  $\epsilon_\perp = 70$  and  $\epsilon_z = 0.1$  in Figure 4a.

To gain a deeper insight, we show the dependence of the critical slab thickness  $d_c$  on both  $\epsilon_\perp$  and  $\epsilon_z$  in Figure 4b. From Figure 4b, the value of  $d_c$  would decrease if  $\epsilon_\perp$  increases, but it is relatively insensitive to the variation of  $\epsilon_z$ . That is, the critical slab thickness that enables the appearance of the ultra-directional transition radiation with enhanced intensity could be engineered on demand via the judicious choice of  $\epsilon_\perp$ . Particularly, the critical slab thickness could be two orders of magnitude smaller than the working wavelength, when  $\epsilon_\perp$  is larger than  $2.4 \times 10^3$  in Figure 4b. For example, we have  $d_c/\lambda_0 = 0.9 \times 10^{-2}$ , if  $\epsilon_\perp = 10^3$  and  $\epsilon_z = 0.1$ .

Counterintuitively, we further show in Figure 4c that when this critical slab thickness is in the deep-subwavelength scale (e.g.,  $d_c/\lambda_0 = 0.9 \times 10^{-2}$ ), the directionality of transition radiation, including the angular width  $\Delta\theta = 0.8^\circ$  and the peak angle  $\theta_p = 7.3^\circ$ , could be insensitive to the variation of electron velocity. This phenomenon is to some extent similar to the phenomenon of free-electron Brewster-transition radiation revealed in Ref., [63] whose radiation peak always appears at the Brewster angle, irrespective of the electron velocity. However, the occurrence of Brewster-transition radiation requires the existence of optical gain and the thickness of the gain slab much larger than the working wave-

length (i.e.,  $d/\lambda_0 \gg 1$ ). On the other hand, Ref. [8] recently reported the phenomenon of low-velocity-favored transition radiation and found that the angular spectral energy density  $U(\theta)$  of this low-velocity-favored transition radiation from hexagonal boron nitrides (*hBN*) is also insensitive to the variation of electron velocity. However, the low-velocity-favored transition radiation in Ref. [87] generally has a very large angular width (e.g.,  $\Delta\theta > 40^\circ$ ). The underlying reason is that for *hBN* (a typical uniaxial epsilon-near-zero material), the value of  $\epsilon_\perp$  is relatively small (i.e.,  $\epsilon_{\perp,hBN} = 7.7$ ) at the frequency of  $\epsilon_z \rightarrow 0$ . Accordingly, we have  $\epsilon_{\perp,hBN} \ll \epsilon_{\perp,c}$  in Ref., [67] which thus cannot enable the emergence of ultra-directional transition radiation with enhanced intensity revealed in this work.

### 3. Discussion

In conclusion, we have revealed a theoretical route to create the ultra-directional transition radiation with enhanced intensity from a deep-subwavelength slab by exploiting anisotropic epsilon-near-zero metamaterials. That is, the anisotropic epsilon-near-zero metamaterial should have one component of the relative permittivity close to zero, but the other components much larger than unity. Moreover, we have found the existence of the critical slab thickness that enables the emergence of ultra-directional transition radiation with enhanced intensity and have further shown that the critical thickness could be reduced down to the unprecedented scale (e.g., one hundred of the working wavelength), through the judicious design of metamaterials' anisotropy. Our theoretical finding thus shows the enticing capability of anisotropic epsilon-near-zero metamaterials in the flexible manipulation of free-electron radiation, including both its directionality and intensity. These anisotropic epsilon-near-zero metamaterials might further pave the way toward the pursuit of novel integrated photonic devices driven by free electrons, such as compact light sources and miniaturized particle detectors. Yet in turn, this enticing pursuit fundamentally relies on the flexible synthesis of epsilon-near-zero metamaterials with the desired permittivity. For example, the extreme anisotropy required by our proposed route to directional transition radiation is seemingly hard to find in natural epsilon-near-zero materials, but could potentially be achieved using an effective-medium approach. Extra care is also needed in a practical experimental setup to avoid the inelastic scattering of the free electron when passing through the sample, which could significantly attenuate the transition-radiation signal. Looking forward, due to the recent emergence of novel photonic nanostructures (e.g., metamaterials, metasurfaces, van der Waals heterostructures, photonic twisted structures, photonic crystals, and spatio-temporal materials), our finding also indicates rich unexplored physics in the realm of light-particle-matter interactions and might stimulate the continual exploration of free-electron radiation in these novel photonic nanostructures.

### 4. Experimental Section

*Derivation of Transition Radiation:* Based on Ginzburg and Frank's theory of transition radiation, we rigorously calculate the angular spectral energy density of transition radiation from a uniaxial metamaterial slab in Figure S1 (Supporting Information). Detailed derivation is provided in

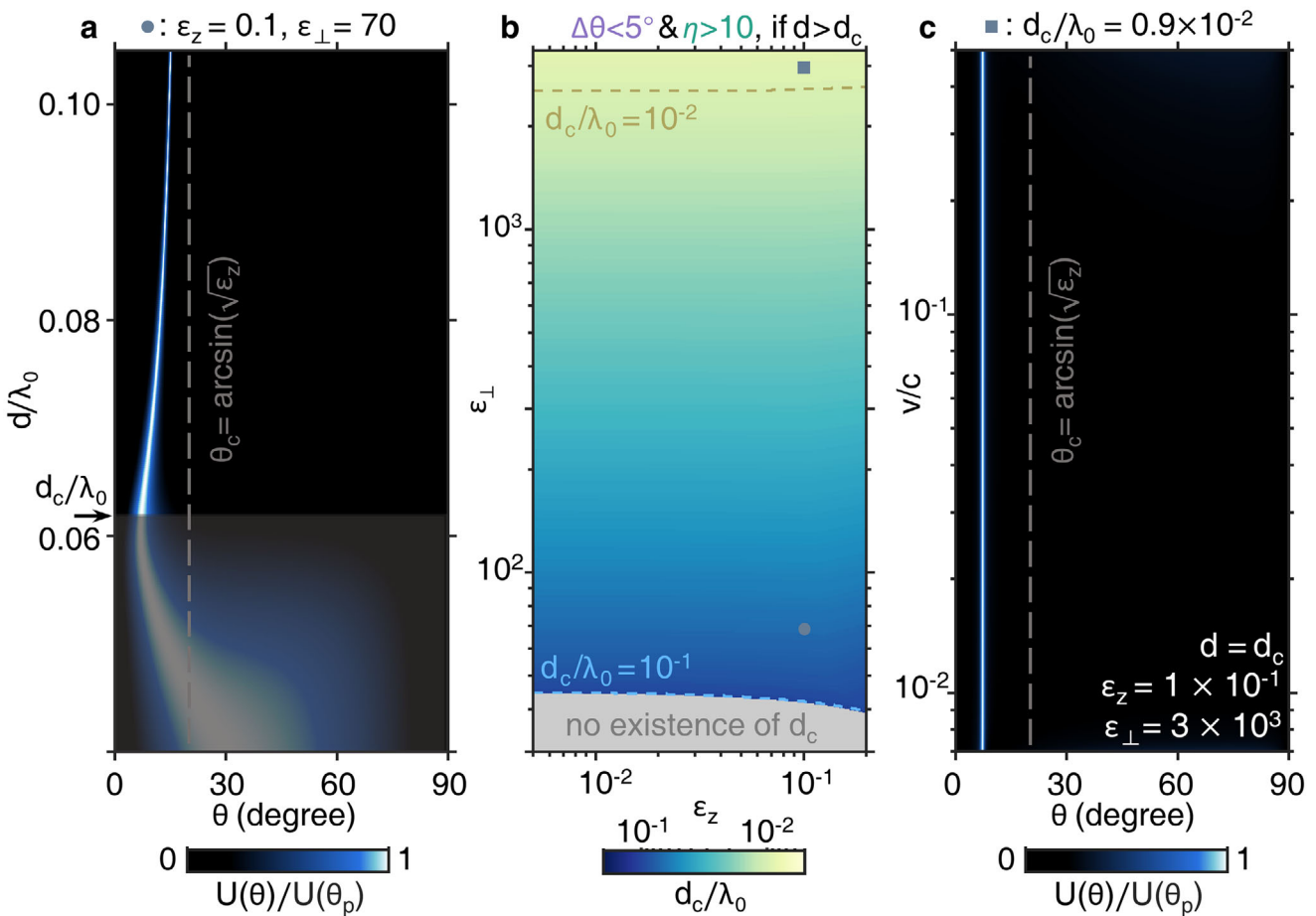


**Figure 4.** Ultra-directional transition radiation from deep-subwavelength anisotropic metamaterial slabs and its dependence on the electron velocity. a) Normalized angular spectral energy density  $U(\theta)/U(\theta_p)$  of emitted light in the  $\theta - d$  parameter space. When the slab thickness  $d$  is larger than the critical value  $d_c$  (i.e.,  $d \geq d_c$ ), we always have  $\Delta\theta \leq 5^\circ$  and  $\eta \geq 10$ . b) Dependence of the critical slab thickness  $d_c$  on  $\epsilon_\perp$  and  $\epsilon_z$ . The value of  $d_c$  is sensitive to the variation of  $\epsilon_\perp$  and is relatively insensitive to the variation of  $\epsilon_z$ . If  $\epsilon_\perp \gg 1$ , the critical slab thickness could be two orders of magnitude smaller than the working wavelength (e.g.,  $d_c/\lambda_0 = 0.9 \times 10^{-2}$ , when  $\epsilon_z = 0.1$  and  $\epsilon_\perp = 3 \times 10^3$ ). c) Normalized angular spectral energy density  $U(\theta)/U(\theta_p)$  of emitted light in the  $\theta - v$  parameter space, under the scenario of  $d_c/\lambda_0 < 10^{-2}$ .

Supporting Section S1 (Supporting Information). After some calculations, the total angular spectral energy density of transition radiation is obtained as  $U(\theta) = (|A_1|^2 + |A_3|^2) \cdot 16\pi^3\omega^2\epsilon_\perp^{3/2}\mu_0^{1/2}\cos^2\theta/\sin^2\theta$ , where  $A_1$  ( $A_3$ ) is the generalized radiation factor in the top (bottom) vacuum region.

**Photonic Density of States of Anisotropic Epsilon-Near-Zero Metamaterials:** The number of photonic eigenmodes per unit volume per frequency (i.e., photonic density of states) is analytically obtained in Supporting Section S2 (Supporting Information), by following the wisdom of condensed physics. The photonic density of states of anisotropic epsilon-near-zero metamaterials that could safely couple into free space is compared with that of isotropic materials in Figure S2 (Supporting Information).

**More Discussion on the Ultra-Directional Transition Radiation From Deep-Subwavelength Epsilon-Near-Zero Metamaterials:** We provide a more detailed discussion on the revealed ultra-directional transition radiation with enhanced intensity in Supporting Section S3 (Supporting Information). The discussion mainly includes possible experimental implementation of the epsilon-near-zero metamaterial required for the emergence of directional transition radiation in Figures S3–S5 (Supporting Information), analysis on transition radiation from various types of epsilon-near-zero metamaterials in Figure S6 (Supporting Information), influence of material loss on the performance of the ultra-directional transition radiation in Figure S7 (Supporting Information), demonstration of special phase vari-

ation of transition radiation inside the epsilon-near-zero metamaterial in Figure S8 (Supporting Information).

## Supporting Information

Supporting Information is available from the Wiley Online Library or from the author.

## Acknowledgements

X.L. acknowledges the support partly from the Fundamental Research Funds for the Central Universities under Grant No. 226-2024-00022, the National Natural Science Foundation of China (NSFC) under Grant No. 62475227 and No. 62175212, and Zhejiang Provincial Natural Science Fund Key Project under Grant No. LZ23F050003. H.C. acknowledges the support from the Key Research and Development Program of the Ministry of Science and Technology under Grants No. 2022YFA1404704, 2022YFA1405200, and 2022YFA1404902, the Key Research and Development Program of Zhejiang Province under Grant No. 2022C01036, and the Fundamental Research Funds for the Central Universities. R.C. acknowledges the support from the National Natural Science Foundation of China

(NSFC) under Grant No. 623B2089. Y.Y. acknowledges the support from the National Natural Science Foundation of China Excellent Young Scientists Fund (12222417), the Hong Kong Research Grants Council through Early Career Scheme (27300924), Strategic Topics (STG3/E-704/23-N), and the Startup Fund of The University of Hong Kong.

## Conflict of interest

The authors have no conflicts to disclose.

## Author Contributions

Z.W. and Z.G. contributed equally to this work. Z.W., Z.G., and X.L. initiated the idea. Z.W. and Z.G. performed the calculation. R.C., X.X., J.C., Y.Y., H.C., and I.K. helped to analyze data and interpret detailed results; Z.W., Z.G., and X.L. wrote the manuscript. X.L., I.K., and H.C. supervised the project.

## Data Availability Statement

The data that support the findings of this study are openly available in Zenodo at [DOI], reference number 16787458.

## Keywords

anisotropic metamaterials, epsilon-near-zero materials, free-electron radiation, light-matter interactions, on-chip light sources

Received: May 7, 2025

Revised: November 6, 2025

Published online:

- [1] V. L. Ginzburg, *Transition Radiation and Transition Scattering*, IOP Publishing Ltd, Hilger 1990.
- [2] G. M. Garibyan, *JETP (USSR)* **1959**, 37, 527.
- [3] F. J. García de Abajo, *Rev. Mod. Phys.* **2010**, 82, 209.
- [4] X. Lin, H. Chen, *Light: Sci. Appl.* **2023**, 12, 187.
- [5] C. Roques-Carmes, S. E. Kooi, Y. Yang, N. Rivera, P. D. Keathley, J. D. Joannopoulos, S. G. Johnson, I. Kaminer, K. K. Berggren, M. Soljacic, *Appl. Phys. Rev.* **2023**, 10, 011303.
- [6] R. Chen, Z. Gong, J. Chen, X. Zhang, X. Zhu, H. Chen, X. Lin, *Mater. Today Electron.* **2023**, 3, 100025.
- [7] B. Dolgoshein, *Nucl. Instrum. Methods Phys. Res., Sect. A* **1993**, 326, 434.
- [8] X. Lin, S. Easo, Y. Shen, H. Chen, B. Zhang, J. D. Joannopoulos, M. Soljacic, I. Kaminer, *Nat. Phys.* **2018**, 14, 816.
- [9] F. Barbosa, H. Fenker, S. Furletov, Y. Furletova, K. Gnanyo, N. Liyanage, L. Pentchev, M. Posik, C. Stanislav, B. Surrow, B. Zühlmann, *Nucl. Instrum. Methods Phys. Res., Sect. A* **2019**, 942, 162356.
- [10] K. D. de Vries, S. Prohira, *Phys. Rev. Lett.* **2019**, 123, 091102.
- [11] J. Déchard, A. Debaille, X. Davoine, L. Gremillet, L. Bergé, *Phys. Rev. Lett.* **2018**, 120, 144801.
- [12] X. Xu, D. B. Cesar, S. Corde, V. Yakimenko, M. J. Hogan, C. Joshi, A. Marinelli, W. B. Mori, *Phys. Rev. Lett.* **2021**, 126, 094801.
- [13] V. M. Grichine, *Nucl. Instrum. Methods Phys. Res., Sect. A* **2022**, 1027, 166322.
- [14] P. Genevet, D. Wintz, A. Ambrosio, A. She, R. Blanchard, F. Capasso, *Nat. Nanotechnol.* **2015**, 10, 804.
- [15] H. Hu, X. Lin, D. Liu, H. Chen, B. Zhang, Y. Luo, *Adv. Sci.* **2022**, 9, 2200538.
- [16] Y. Adiv, H. Hu, S. Tsesses, R. Dahan, K. Wang, Y. Kurman, A. Gorlach, H. Chen, X. Lin, G. Bartal, I. Kaminer, *Phys. Rev. X* **2023**, 13, 011002.
- [17] X. Guo, C. Wu, S. Zhang, D. Hu, S. Zhang, Q. Jiang, X. Dai, Y. Duan, X. Yang, Z. Sun, S. Zhang, H. Xu, Q. Dai, *Nat. Commun.* **2023**, 14, 2532.
- [18] H. Hu, X. Lin, G. Hu, F. J. Garcia-Vidal, Y. Luo, *InfoScience* **2024**, 2, 12024.
- [19] R. Yu, S. Fan, *Nano Lett.* **2024**, 25, 529.
- [20] R. Chen, Z. Gong, Z. Wang, X. Xi, B. Zhang, Y. Yang, B. Zhang, I. Kaminer, H. Chen, X. Lin, *Sci. Adv.* **2025**, 11, ads5113.
- [21] C. Luo, M. Ibanescu, S. G. Johnson, J. D. Joannopoulos, *Science* **2003**, 299, 368.
- [22] F. Liu, L. Xiao, Y. Ye, M. Wang, K. Cui, X. Feng, W. Zhang, Y. Huang, *Nat. Photonics* **2017**, 11, 289.
- [23] H. Hu, X. Lin, J. Zhang, D. Liu, P. Genevet, B. Zhang, Y. Luo, *Laser Photonics Rev.* **2020**, 14, 2000149.
- [24] Z. Gong, J. Chen, R. Chen, X. Zhu, C. Wang, X. Zhang, H. Hu, Y. Yang, B. Zhang, H. Chen, I. Kaminer, X. Lin, *Proc. Natl. Acad. Sci. USA* **2023**, 120, 2306601120.
- [25] Z. Duan, X. Tang, Z. Wang, Y. Zhang, X. Chen, M. Chen, Y. Gong, *Nat. Commun.* **2017**, 8, 14901.
- [26] T. M. Shaffer, E. C. Pratt, J. Grimm, *Nat. Nanotechnol.* **2017**, 12, 106.
- [27] H. Hu, X. Lin, L. J. Wong, Q. Yang, D. Liu, B. Zhang, Y. Luo, *eLight* **2022**, 2, 2.
- [28] X. Lin, H. Hu, S. Easo, Y. Yang, Y. Shen, K. Yin, M. P. Blago, I. Kaminer, B. Zhang, H. Chen, J. Joannopoulos, M. Soljacic, Y. Luo, *Nat. Commun.* **2021**, 12, 5554.
- [29] G. dos Santos Ilha, M. Boix, J. Knöldlseder, P. Garnier, L. Montastruc, P. Jean, G. Pareschi, A. Steiner, F. Toussenel, *Nat Astron.* **2024**, 8, 1468.
- [30] Z. Xu, S. Bao, J. Liu, J. Chang, X. Kong, V. Galdi, T. J. Cui, *Laser Photonics Rev.* **2024**, 18, 2300763.
- [31] G. Liu, W. Chen, Z. Xiong, Y. Wang, S. Zhang, Z. Xia, *Nat. Photonics* **2024**, 18, 562.
- [32] A. P. Synanidis, P. A. D. Gonçalves, C. Ropers, F. J. García de Abajo, *Sci. Adv.* **2024**, 10, adp4096.
- [33] A. Andronic, J. P. Wessels, *Nucl. Instrum. Methods Phys. Res., Sect. A* **2012**, 666, 130.
- [34] P. Du, D. Egana-Ugrinovic, R. Essig, M. Sholapurkar, *Phys. Rev. X* **2022**, 12, 011009.
- [35] L. J. Wong, I. Kaminer, O. Ilic, J. D. Joannopoulos, M. Soljačić, *Nat. Photonics* **2016**, 10, 46.
- [36] S. Huang, R. Duan, N. Pramanik, C. Boothroyd, Z. Liu, L. J. Wong, *Adv. Sci.* **2022**, 9, 2105401.
- [37] X. Shi, Y. Kurman, M. Shentcis, L. J. Wong, F. J. García de Abajo, I. Kaminer, *Light: Sci. Appl.* **2023**, 12, 148.
- [38] X.-Q. Yu, Y.-S. Zeng, L.-W. Song, D.-Y. Kong, S.-B. Hao, J.-Y. Gui, X.-J. Yang, Y. Xu, X.-J. Wu, Y.-X. Leng, Y. Tian, R.-X. Li, *Nat. Photonics* **2023**, 17, 957.
- [39] Y. Yang, C. Roques-Carmes, S. E. Kooi, H. Tang, J. Beroz, E. Mazur, I. Kaminer, J. D. Joannopoulos, M. Soljacic, *Nature* **2023**, 613, 42.
- [40] A. Polman, M. Kociak, F. J. García de Abajo, *Nat. Mater.* **2019**, 18, 1158.
- [41] C. Wang, X. Chen, Z. Gong, R. Chen, H. Hu, H. Wang, Y. Yang, L. Tony, B. Zhang, H. Chen, X. Lin, *Rep. Prog. Phys.* **2024**, 87, 126401.
- [42] Z. Gong, R. Chen, H. Chen, X. Lin, *Appl. Phys. Rev.* **2025**, 12, 3.
- [43] X. Shi, W. W. Lee, A. Karnieli, L. M. Lohse, A. Gorlach, L. W. W. Wong, T. Saldit, S. Fan, I. Kaminer, L. J. Wong, *Prog. Quantum Electron.* **2025**, 102, 100577.
- [44] X. Lin, I. Kaminer, X. Shi, F. Gao, Z. Yang, Z. Gao, H. Buljan, J. D. Joannopoulos, M. Soljacic, H. Chen, B. Zhang, *Sci. Adv.* **2017**, 3, 1601192.
- [45] J. Chen, X. Lin, H. Chen, *J. Opt.* **2021**, 23, 034001.
- [46] K. Akbari, Z. L. Mišković, *Nanoscale* **2022**, 14, 5079.

- [47] D. Zhang, Y. Zeng, Y. Bai, Z. Li, Y. Tian, R. Li, *Nature* **2022**, *611*, 55.
- [48] F. Tay, X. Lin, X. Shi, H. Chen, I. Kaminer, B. Zhang, *Adv. Sci.* **2023**, *10*, 2300760.
- [49] J. Chen, X. Lin, M. Chen, T. Low, H. Chen, S. Dai, *Appl. Phys. Lett.* **2021**, *119*, 240501.
- [50] A. Dikopoltsev, Y. Sharabi, M. Lyubarov, Y. Lumer, S. Tsesses, E. Lustig, I. Kaminer, M. Segev, *Proc. Natl. Acad. Sci. USA* **2022**, *119*, 2119705119.
- [51] X. Zheng, J. Lin, Z. Wang, H. Zhou, Q. He, L. Zhou, *PhotoniX* **2023**, *4*, 3.
- [52] P. Lin, C. Qian, J. Zhang, J. Chen, X. Zhu, Z. Wang, J. Huangfu, H. Chen, *Prog. Electromagn. Res.* **2023**, *178*, 83.
- [53] T. J. Cui, S. Zhang, A. Alù, M. Wegener, *J. Phys.: Photon.* **2024**, *6*, 032502.
- [54] S. A. Schulz, R. F. Oulton, M. Kenney, A. Alù, I. Staude, A. Bashiri, Z. Fedorova, R. Kolkowski, A. F. Koenderink, X. Xiao, J. Yang, W. J. Peveler, A. W. Clark, G. Perrakis, A. C. Tasolamprou, M. Kafesaki, A. Zaleska, W. Dickson, D. Richards, A. Zayats, H. Ren, Y. Kivshar, S. Maier, X. Chen, M. A. Ansari, Y. Gan, A. Alexeev, T. F. Krauss, A. Di Falco, S. D. Gennaro, et al., *Appl. Phys. Lett.* **2024**, *124*, 260701.
- [55] R. Ballabriga, M. Campbell, X. Llopart, *Nucl. Instrum. Methods Phys. Res., Sect. A* **2018**, *878*, 10.
- [56] J. Liu, W. Yang, G. Song, Q. Gan, *PhotoniX* **2023**, *4*, 1.
- [57] G. Adamo, K. F. MacDonald, Y. H. Fu, C.-M. Wang, D. P. Tsai, F. J. García de Abajo, N. I. Zheludev, *Phys. Rev. Lett.* **2009**, *103*, 113901.
- [58] J.-W. Henke, A. S. Raja, A. Feist, G. Huang, G. Arend, Y. Yang, F. J. Kappert, R. N. Wang, M. Möller, J. Pan, J. Liu, O. Kfir, C. Ropers, T. J. Kippenberg, *Nature* **2021**, *600*, 653.
- [59] Y. Yang, J.-W. Henke, A. S. Raja, F. J. Kappert, G. Huang, G. Arend, Z. Qiu, A. Feist, R. N. Wang, A. Tusnin, A. Tikan, C. Ropers, T. J. Kippenberg, *Science* **2024**, *383*, 168.
- [60] M. A. Piestrup, D. G. Boyers, C. I. Pincus, J. L. Harris, J. C. Bergstrom, H. S. Caplan, R. M. Silzer, D. M. Skopik, *Appl. Phys. Lett.* **1991**, *58*, 2692.
- [61] G.-Q. Liao, Y.-T. Li, Y.-H. Zhang, H. Liu, X.-L. Ge, S. Yang, W.-Q. Wei, X.-H. Yuan, Y.-Q. Deng, B.-J. Zhu, Z. Zhang, W.-M. Wang, Z.-M. Sheng, L.-M. Chen, X. Lu, J.-L. Ma, X. Wang, J. Zhang, *Phys. Rev. Lett.* **2016**, *116*, 205003.
- [62] Y. Yu, K. Lai, J. Shao, J. Power, M. Conde, W. Liu, S. Doran, C. Jing, E. Wisniewski, G. Shvets, *Phys. Rev. Lett.* **2019**, *123*, 057402.
- [63] R. Chen, J. Chen, Z. Gong, X. Zhang, X. Zhu, Y. Yang, I. Kaminer, H. Chen, B. Zhang, X. Lin, *Sci. Adv.* **2023**, *9*, adh8098.
- [64] K. Shastri, O. Reshef, R. W. Boyd, J. S. Lundeen, F. Monticone, *Optica* **2022**, *9*, 738.
- [65] D. A. Miller, *Science* **2023**, *379*, 41.
- [66] Y. Tian, J. Liu, Y. Bai, S. Zhou, H. Sun, W. Liu, J. Zhao, R. Li, Z. Xu, *Nat. Photonics* **2017**, *11*, 242.
- [67] K. Wang, R. Dahan, M. Shentcis, Y. Kauffmann, A. Ben Hayun, O. Reinhardt, S. Tsesses, I. Kaminer, *Nature* **2020**, *582*, 50.
- [68] H. Hu, X. Lin, Y. Luo, *Prog. Electromagn. Res.* **2021**, *171*, 75.
- [69] L. Jing, X. Lin, Z. Wang, I. Kaminer, H. Hu, E. Li, Y. Liu, M. Chen, B. Zhang, H. Chen, *Laser Photonics Rev.* **2021**, *15*, 2000426.
- [70] R. Dahan, G. Baranes, A. Gorlach, R. Ruimy, N. Rivera, I. Kaminer, *Phys. Rev. X* **2023**, *13*, 031001.
- [71] S. Huang, R. Duan, N. Pramanik, M. Go, C. Boothroyd, Z. Liu, L. J. Wong, *Sci. Adv.* **2023**, *9*, adj8584.
- [72] M. Labat, J. C. Cabadag, A. Ghaith, A. Irman, A. Berlioux, P. Berteaud, F. Blache, S. Bock, F. Bouvet, F. Briquet, Y.-Y. Chang, S. Corde, A. Debus, C. De Oliveira, J.-P. Duval, Y. Dietrich, M. El Ajjouri, C. Eisenmann, J. Gautier, R. Gebhardt, S. Grams, U. Helbig, C. Herbeaux, N. Hubert, C. Kitagi, O. Kononenko, M. Kuntzsch, M. LaBerge, S. Lê, B. Leluan, et al., *Nat. Photonics* **2023**, *17*, 150.
- [73] A. Polman, F. J. García de Abajo, *Science* **2024**, *383*, 148.
- [74] N. Pramanik, S. Huang, R. Duan, Q. Zhai, M. Go, C. Boothroyd, Z. Liu, L. J. Wong, *Nat. Photonics* **2024**, *18*, 1203.
- [75] Z. Gong, R. Chen, Z. Wang, X. Xi, Y. Yang, B. Zhang, H. Chen, I. Kaminer, X. Lin, *Proc. Natl. Acad. Sci. USA* **2025**, *122*, 2413336122.
- [76] R. A. Ferrell, *Phys. Rev.* **1958**, *111*, 1214.
- [77] J. Wu, Z. T. Xie, Y. Sha, H. Y. Fu, Q. Li, *Photonics Res.* **2021**, *9*, 1616.
- [78] Y. Li, C. T. Chan, E. Mazur, *Light: Sci. Appl.* **2021**, *10*, 203.
- [79] M. Lobet, N. Kinsey, I. Liberal, H. Caglayan, P. A. Huidobro, E. Galiffi, J. R. Mejía-Salazar, G. Palermo, Z. Jacob, N. Maccaferri, *ACS Photonics* **2023**, *10*, 3805.
- [80] G. E. Lio, A. Ferraro, R. Kowerdziej, A. O. Govorov, Z. Wang, R. Caputo, *Adv. Opt. Mater.* **2023**, *11*, 2203123.
- [81] G. E. Lio, A. Ferraro, B. Zappone, J. Parka, E. Schab-Balcerzak, C. P. Umeton, F. Riboli, R. Kowerdziej, R. Caputo, *Adv. Opt. Mater.* **2024**, *12*, 2302483.
- [82] D. Formra, A. Ball, S. Saha, J. Wu, M. Sojib, A. Agrawal, H. J. Lezec, N. Kinsey, *Appl. Phys. Rev.* **2024**, *11*, 011317.
- [83] W. Steinmann, *Phys. Rev. Lett.* **1960**, *5*, 470.
- [84] V. P. Silin, E. P. Fetisov, *Phys. Rev. Lett.* **1961**, *7*, 374.
- [85] E. A. Stern, *Phys. Rev. Lett.* **1962**, *8*, 7.
- [86] F. J. García de Abajo, M. Kociak, *Phys. Rev. Lett.* **2008**, *100*, 106804.
- [87] J. Chen, R. Chen, F. Tay, Z. Gong, H. Hu, Y. Yang, X. Zhang, C. Wang, I. Kaminer, H. Chen, B. Zhang, X. Lin, *Phys. Rev. Lett.* **2023**, *131*, 113002.

**Supplementary information for**  
**Ultra-directional transition radiation**  
**from deep-subwavelength epsilon-near-zero metamaterials**

Zun Wang, Zheng Gong, Ruoxi Chen, Xiangfeng Xi, Jialin Chen, Yi Yang, Hongsheng Chen, Erping Li,  
Ido Kaminer, and Xiao Lin

**Supplementary Information Guide:**

**Section S1. Derivation of transition radiation**

- S1.1 Transition radiation from uniaxial slab
- S1.2 Angular spectral energy density of transition radiation

**Section S2. Photonic density of states of anisotropic epsilon-near-zero metamaterials**

**Section S3. More discussion on the ultra-directional transition radiation from deep-subwavelength epsilon-near-zero metamaterials**

- S3.1 Possible experimental implementation of the epsilon-near-zero metamaterial required for the emergence of directional transition radiation
- S3.2 Transition radiation from various types of epsilon-near-zero metamaterials
- S3.3 Influence of material loss on the performance of the ultra-directional transition radiation
- S3.4 Special phase variation of transition radiation inside the epsilon-near-zero metamaterial

**Reference**

## Section S1. Derivation of transition radiation

### S1.1 Transition radiation from uniaxial slab

In this section, we derive the transition radiation from a uniaxial metamaterial based on the theory of transition radiation proposed by Ginzburg and Frank. As shown in Figure S1a, when an electron with charge  $q$  and velocity  $\bar{v}$  traverses a single interface perpendicularly along the  $+\hat{z}$  direction, transition radiation occurs in both the backward and forward directions. On this basis, we examine the transition radiation emitted from a uniaxial metamaterial slab with thickness  $d$ , as depicted in Figure S1b. This metamaterial slab in region 2 is surrounded by vacuum on its top (region 1) and bottom (region 3) and has a relative permittivity tensor  $\bar{\epsilon}_{r2} = [\epsilon_{\perp}, \epsilon_{\perp}, \epsilon_z]$ .

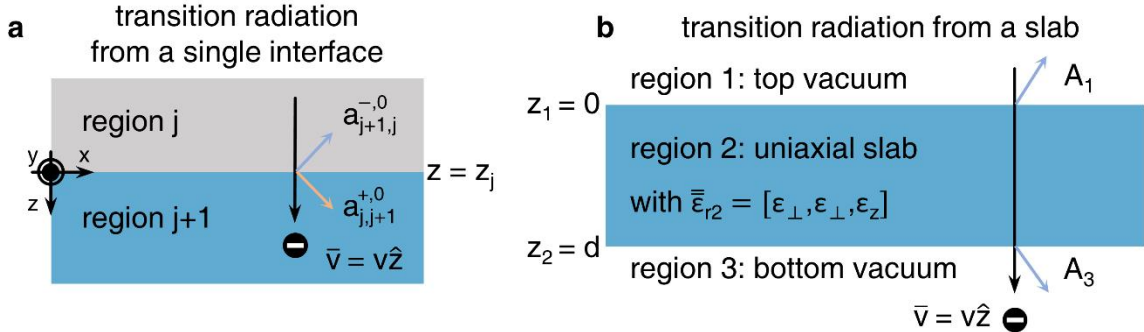


**Figure S1.** Schematic of transition radiation. (a) Transition radiation from a single interface. (b) Transition radiation from a uniaxial slab.

From the Maxwell's electromagnetic theory, the induced current density from the moving electron is

$$\bar{J}^q(\bar{r}, t) = \hat{z} q v \delta(x) \delta(y) \delta(z - vt) \quad (S1)$$

By performing Fourier transformation, equation (S1) can be expressed as

$$\bar{J}^q(\bar{r}, t) = \hat{z} \int d\omega \int d\bar{k}_\perp J_{\bar{k}_\perp, \omega}^q(z) e^{i\bar{k}_\perp \bar{r}_\perp - i\omega t} \quad (S2)$$

where  $\bar{k}_\perp = \hat{x}k_x + \hat{y}k_y$  is the wavevector component perpendicular to the electron velocity and  $\bar{r}_\perp = \hat{x}x + \hat{y}y$ . By combining equations (S1-S2), we have

$$J_{\bar{k}_\perp, \omega}^q(z) = \frac{q}{(2\pi)^3} e^{i\omega z/v} \quad (S3)$$

Similarly, we apply the Fourier transformation to the electric field  $\bar{E}(\bar{r}, t)$  and the magnetic field  $\bar{H}(\bar{r}, t)$ ,

namely

$$\bar{E}(\bar{r}, t) = \hat{z} \int d\omega \int d\bar{k}_\perp \bar{E}_{\bar{k}_\perp, \omega}(z) e^{i\bar{k}_\perp \cdot \bar{r}_\perp - i\omega t} \quad (S4)$$

$$\bar{H}(\bar{r}, t) = \hat{z} \int d\omega \int d\bar{k}_\perp \bar{H}_{\bar{k}_\perp, \omega}(z) e^{i\bar{k}_\perp \cdot \bar{r}_\perp - i\omega t} \quad (S5)$$

After the transformations above, the Helmholtz equations can be written as

$$(\partial^2/\partial z^2 + \omega^2 \mu_0 \epsilon_0 \epsilon_{r1} - k_\perp^2) \begin{pmatrix} E_{z1}(z) \\ H_{z1}(z) \end{pmatrix} = \begin{pmatrix} (\partial^2/\partial z^2 + \omega^2 \mu_0 \epsilon_0 \epsilon_{r1}) & \frac{J}{-i\omega \epsilon_0 \epsilon_{r1}} \\ 0 & 0 \end{pmatrix} \quad (S6)$$

$$(\partial^2/\partial z^2 + \omega^2 \mu_0 \epsilon_0 \epsilon_\perp - k_\perp^2) \begin{pmatrix} E_{z2}(z) \\ H_{z2}(z) \end{pmatrix} = \begin{pmatrix} (\partial^2/\partial z^2 + \omega^2 \mu_0 \epsilon_0 \epsilon_\perp) & \frac{J}{-i\omega \epsilon_0 \epsilon_z} \\ 0 & 0 \end{pmatrix} \quad (S7)$$

$$(\partial^2/\partial z^2 + \omega^2 \mu_0 \epsilon_0 \epsilon_{r3} - k_\perp^2) \begin{pmatrix} E_{z3}(z) \\ H_{z3}(z) \end{pmatrix} = \begin{pmatrix} (\partial^2/\partial z^2 + \omega^2 \mu_0 \epsilon_0 \epsilon_{r3}) & \frac{J}{-i\omega \epsilon_0 \epsilon_{r3}} \\ 0 & 0 \end{pmatrix} \quad (S8)$$

where  $\epsilon_{r1} = \epsilon_{r3} = 1$  are the relative permittivities of the vacuum regions. Then, the solution of  $E_z(z)$  can be expressed as

$$E_z(z) = E_z^q(z) + E_z^R(z) \quad (S9)$$

$$E_{z1}^q = \frac{q[\omega^2 \mu_0 \epsilon_0 \epsilon_{r1} - (\omega/v)^2]}{i\omega \epsilon_0 \epsilon_{r1} (2\pi)^3 [\omega^2 \mu_0 \epsilon_0 \epsilon_{r1} - k_\perp^2 - (\omega/v)^2]} e^{i\omega z/v} \quad (S10)$$

$$E_{z1}^R = A_1 e^{-ik_{z1}z} \quad (S11)$$

$$E_{z2}^q = \frac{q[\omega^2 \mu_0 \epsilon_0 \epsilon_\perp - (\omega/v)^2]}{i\omega \epsilon_0 \epsilon_z (2\pi)^3 [\omega^2 \mu_0 \epsilon_0 \epsilon_\perp - k_\perp^2 \frac{\epsilon_\perp}{\epsilon_z} - (\omega/v)^2]} e^{i\omega z/v} \quad (S12)$$

$$E_{z2}^R = A_2^- e^{-ik_{z2}(z-d)} + A_2^+ e^{ik_{z2}z} \quad (S13)$$

$$E_{z3}^q = \frac{q[\omega^2 \mu_0 \epsilon_0 \epsilon_{r3} - (\omega/v)^2]}{i\omega \epsilon_0 \epsilon_{r3} (2\pi)^3 [\omega^2 \mu_0 \epsilon_0 \epsilon_{r3} - k_\perp^2 - (\omega/v)^2]} e^{i\omega z/v} \quad (S14)$$

$$E_{z3}^R = A_3 e^{ik_{z3}(z-d)} \quad (S15)$$

where  $k_{z1} = \sqrt{\omega^2 \mu_0 \varepsilon_0 \varepsilon_{r1} - k_\perp^2}$ ,  $k_{z2} = \sqrt{\omega^2 \mu_0 \varepsilon_0 \varepsilon_\perp - k_\perp^2 \frac{\varepsilon_\perp}{\varepsilon_z}}$ ,  $k_{z3} = \sqrt{\omega^2 \mu_0 \varepsilon_0 \varepsilon_{r3} - k_\perp^2}$ ,  $A_j$  represents the generalized radiation factor in region  $j$ ,  $E_z^q(z)$  corresponds to the charge field carried by the electron, and  $E_z^R(z)$  corresponds to the radiation field emitted from the interface.

On the basis of equations (S9-S15), we further match the boundary conditions, namely

$$\hat{n} \times (\bar{E}_{\perp 1} - \bar{E}_{\perp 2})|_{z=0} = 0 \quad (S16)$$

$$\hat{n} \times (\bar{H}_{\perp 1} - \bar{H}_{\perp 2})|_{z=0} = 0 \quad (S17)$$

$$\hat{n} \times (\bar{E}_{\perp 2} - \bar{E}_{\perp 3})|_{z=d} = 0 \quad (S18)$$

$$\hat{n} \times (\bar{H}_{\perp 2} - \bar{H}_{\perp 3})|_{z=d} = 0 \quad (S19)$$

By solving equations (S16-S19), one can obtain the radiation factors as

$$A_1 = a_{1,2}^{-,0} + a_{1,2}^{+,0} \frac{T_{21} R_{23} e^{2ik_{z2}d}}{1 - R_{21} R_{23} e^{2ik_{z2}d}} + a_{2,3}^{-,0} \frac{T_{21} e^{ik_{z2}d + i\frac{\omega}{v}d}}{1 - R_{21} R_{23} e^{2ik_{z2}d}} \quad (S20)$$

$$A_2^- = a_{1,2}^{+,0} \frac{R_{23} e^{i2k_{z2}d}}{1 - R_{21} R_{23} e^{2ik_{z2}d}} + a_{2,3}^{-,0} \frac{e^{ik_{z2}d + i\frac{\omega}{v}d}}{1 - R_{21} R_{23} e^{2ik_{z2}d}} \quad (S21)$$

$$A_2^+ = a_{1,2}^{+,0} \frac{1}{1 - R_{21} R_{23} e^{2ik_{z2}d}} + a_{2,3}^{-,0} \frac{R_{21} e^{i2k_{z2}d + i\frac{\omega}{v}d}}{1 - R_{21} R_{23} e^{2ik_{z2}d}} \quad (S22)$$

$$A_3 = a_{2,3}^{+,0} e^{i\frac{\omega}{v}d} + a_{1,2}^{+,0} \frac{T_{23} e^{ik_{z2}d}}{1 - R_{21} R_{23} e^{2ik_{z2}d}} + a_{2,3}^{-,0} \frac{T_{23} R_{21} e^{2ik_{z2}d} e^{i\frac{\omega}{v}d}}{1 - R_{21} R_{23} e^{2ik_{z2}d}} \quad (S23)$$

$$a_{1,2}^{-,0} = \frac{iq}{\omega \varepsilon_0 (2\pi)^3} \frac{\varepsilon_\perp k_\perp^2 \left( \frac{\omega/v - k_{z2}}{\varepsilon_z (k_{z2}^2 - \omega^2/v^2)} - \frac{\omega/v - k_{z2} \varepsilon_{r1}/\varepsilon_\perp}{\varepsilon_{r1} (k_{z1}^2 - \omega^2/v^2)} \right)}{(k_{z2} \varepsilon_{r1} + k_{z1} \varepsilon_\perp)} \quad (S24)$$

$$a_{1,2}^{+,0} = \frac{-iq}{\omega \varepsilon_0 (2\pi)^3} \frac{\varepsilon_\perp k_\perp^2 \left( \frac{\omega/v + k_{z1}}{(k_{z1}^2 - \omega^2/v^2)} - \frac{\varepsilon_{r1} \omega/v + k_{z1} \varepsilon_\perp}{\varepsilon_z (k_{z2}^2 - \omega^2/v^2)} \right)}{\varepsilon_z (k_{z2} \varepsilon_{r1} + k_{z1} \varepsilon_\perp)} \quad (S25)$$

$$a_{2,3}^{-,0} = \frac{iq}{\omega \varepsilon_0 (2\pi)^3} \frac{\varepsilon_\perp k_\perp^2 \left( \frac{\omega/v - k_{z3}}{(k_{z3}^2 - \omega^2/v^2)} - \frac{\varepsilon_{r3} \omega/v - k_{z3} \varepsilon_\perp}{\varepsilon_z (k_{z2}^2 - \omega^2/v^2)} \right)}{\varepsilon_z (k_{z2} \varepsilon_{r3} + k_{z3} \varepsilon_\perp)} \quad (S26)$$

$$a_{2,3}^{+,0} = \frac{-iq}{\omega \varepsilon_0 (2\pi)^3} \frac{\varepsilon_\perp k_\perp^2 \left( \frac{\omega/v + k_{z2}}{\varepsilon_z (k_{z2}^2 - \omega^2/v^2)} - \frac{\omega/v + k_{z2} \varepsilon_{r3}/\varepsilon_\perp}{\varepsilon_{r3} (k_{z3}^2 - \omega^2/v^2)} \right)}{(k_{z2} \varepsilon_{r3} + k_{z3} \varepsilon_\perp)} \quad (S27)$$

where the transmission and reflection coefficients are given by

$$R_{21} = \frac{\frac{k_{z2}}{\varepsilon_\perp} - \frac{k_{z1}}{\varepsilon_{r1}}}{\frac{k_{z2}}{\varepsilon_\perp} + \frac{k_{z1}}{\varepsilon_{r1}}}, T_{21} = \frac{2 \frac{k_{z2}}{\varepsilon_\perp} \frac{\varepsilon_z}{\varepsilon_{r1}}}{\frac{k_{z2}}{\varepsilon_\perp} + \frac{k_{z1}}{\varepsilon_{r1}}} \quad (S28)$$

$$R_{23} = \frac{\frac{k_{z2}}{\varepsilon_\perp} - \frac{k_{z3}}{\varepsilon_{r3}}}{\frac{k_{z2}}{\varepsilon_\perp} + \frac{k_{z3}}{\varepsilon_{r3}}}, T_{23} = \frac{2 \frac{k_{z2}}{\varepsilon_\perp} \frac{\varepsilon_z}{\varepsilon_{r3}}}{\frac{k_{z2}}{\varepsilon_\perp} + \frac{k_{z3}}{\varepsilon_{r3}}} \quad (S29)$$

In all, we can obtain field distribution in all regions as

$$\bar{E}_j(\bar{r}, t) = \bar{E}_j^q(\bar{r}, t) + \bar{E}_j^R(\bar{r}, t) \quad (S30)$$

$$\begin{aligned} \bar{E}_1^q(\bar{r}, t) &= \hat{z} \int_{-\infty}^{+\infty} d\omega \frac{-q}{8\pi\omega\varepsilon_0\varepsilon_{r1}} (\omega^2\mu_0\varepsilon_0\varepsilon_{r1} - \omega^2/v^2) H_0^{(1)}(\sqrt{\omega^2\mu_0\varepsilon_0\varepsilon_{r1} - \omega^2/v^2}\rho) e^{i\omega z/v - i\omega t} \\ &\quad + \hat{\rho} \int_{-\infty}^{+\infty} d\omega \frac{iq}{8\pi\nu\varepsilon_0\varepsilon_{r1}} \sqrt{\omega^2\mu_0\varepsilon_0\varepsilon_{r1} - \omega^2/v^2} H_1^{(1)}(\sqrt{\omega^2\mu_0\varepsilon_0\varepsilon_{r1} - \omega^2/v^2}\rho) e^{i\omega z/v - i\omega t} \end{aligned} \quad (S31)$$

$$\begin{aligned} \bar{E}_2^q(\bar{r}, t) &= \hat{z} \int_{-\infty}^{+\infty} d\omega \frac{-q}{8\pi\omega\varepsilon_0\varepsilon_\perp} (\omega^2\mu_0\varepsilon_0\varepsilon_\perp - \omega^2/v^2) H_0^{(1)}(\sqrt{\omega^2\mu_0\varepsilon_0\varepsilon_\perp - \omega^2/v^2}\rho) e^{i\omega z/v - i\omega t} \\ &\quad + \hat{\rho} \int_{-\infty}^{+\infty} d\omega \frac{iq}{8\pi\nu\varepsilon_0\varepsilon_\perp} \sqrt{\omega^2\mu_0\varepsilon_0\varepsilon_\perp - \omega^2/v^2} H_1^{(1)}(\sqrt{\omega^2\mu_0\varepsilon_0\varepsilon_\perp - \omega^2/v^2}\rho) e^{i\omega z/v - i\omega t} \end{aligned} \quad (S32)$$

$$\begin{aligned} \bar{E}_3^q(\bar{r}, t) &= \hat{z} \int_{-\infty}^{+\infty} d\omega \frac{-q}{8\pi\omega\varepsilon_0\varepsilon_{r3}} (\omega^2\mu_0\varepsilon_0\varepsilon_{r3} - \omega^2/v^2) H_0^{(1)}(\sqrt{\omega^2\mu_0\varepsilon_0\varepsilon_{r3} - \omega^2/v^2}\rho) e^{i\omega z/v - i\omega t} \\ &\quad + \hat{\rho} \int_{-\infty}^{+\infty} d\omega \frac{iq}{8\pi\nu\varepsilon_0\varepsilon_{r3}} \sqrt{\omega^2\mu_0\varepsilon_0\varepsilon_{r3} - \omega^2/v^2} H_1^{(1)}(\sqrt{\omega^2\mu_0\varepsilon_0\varepsilon_{r3} - \omega^2/v^2}\rho) e^{i\omega z/v - i\omega t} \end{aligned} \quad (S33)$$

$$\begin{aligned} \bar{E}_1^R(\bar{r}, t) &= \hat{z} \int_{-\infty}^{+\infty} d\omega \int_0^{+\infty} dk_\perp A_1 k_\perp 2\pi J_0(k_\perp\rho) e^{-ik_{z1}z - i\omega t} \\ &\quad + \hat{\rho} \int_{-\infty}^{+\infty} d\omega \int_0^{+\infty} dk_\perp i A_1 k_{z1} 2\pi J_1(k_\perp\rho) e^{-ik_{z1}z - i\omega t} \end{aligned} \quad (S34)$$

$$\begin{aligned} \bar{E}_2^R(\bar{r}, t) &= \hat{z} \int_{-\infty}^{+\infty} d\omega \int_0^{+\infty} dk_\perp k_\perp 2\pi J_0(k_\perp\rho) (A_2^- e^{-ik_{z2}(z-d)} + A_2^+ e^{ik_{z2}z}) e^{-i\omega t} \\ &\quad + \hat{\rho} \int_{-\infty}^{+\infty} d\omega \int_0^{+\infty} dk_\perp i k_{z2} 2\pi J_1(k_\perp\rho) (A_2^- e^{-ik_{z2}(z-d)} + A_2^+ e^{ik_{z2}z}) e^{-i\omega t} \end{aligned} \quad (S35)$$

$$\begin{aligned} \bar{E}_3^R(\bar{r}, t) &= \hat{z} \int_{-\infty}^{+\infty} d\omega \int_0^{+\infty} dk_\perp A_3 k_\perp 2\pi J_0(k_\perp\rho) e^{ik_{z3}z - i\omega t} \\ &\quad + \hat{\rho} \int_{-\infty}^{+\infty} d\omega \int_0^{+\infty} dk_\perp -i A_3 k_{z3} 2\pi J_1(k_\perp\rho) e^{ik_{z3}z - i\omega t} \end{aligned} \quad (S36)$$

$$\bar{H}_j(\bar{r}, t) = \bar{H}_j^q(\bar{r}, t) + \bar{H}_j^R(\bar{r}, t) \quad (S37)$$

$$\bar{H}_1^q(\bar{r}, t) = \hat{\varphi} \int_{-\infty}^{+\infty} d\omega \frac{iq\omega}{8\pi} \sqrt{\mu_0\varepsilon_0\varepsilon_{r1} - 1/v^2} H_1^{(1)}(\sqrt{\omega^2\mu_0\varepsilon_0\varepsilon_{r1} - \omega^2/v^2}\rho) e^{i\omega z/v - i\omega t} \quad (S38)$$

$$\bar{H}_2^q(\bar{r}, t) = \hat{\varphi} \int_{-\infty}^{+\infty} d\omega \frac{iq\omega}{8\pi} \sqrt{\mu_0\varepsilon_0\varepsilon_z - \varepsilon_z/(\varepsilon_\perp v^2)} H_1^{(1)}(\sqrt{\omega^2\mu\varepsilon_0\varepsilon_z - (\varepsilon_z\omega^2)/(\varepsilon_\perp v^2)}\rho) e^{i\omega z/v - i\omega t} \quad (S39)$$

$$\bar{H}_3^q(\bar{r}, t) = \hat{\varphi} \int_{-\infty}^{+\infty} d\omega \frac{iq\omega}{8\pi} \sqrt{\mu_0\varepsilon_0\varepsilon_{r3} - 1/v^2} H_1^{(1)}(\sqrt{\omega^2\mu_0\varepsilon_0\varepsilon_{r3} - \omega^2/v^2}\rho) e^{i\omega z/v - i\omega t} \quad (S40)$$

$$\bar{H}_1^R(\bar{r}, t) = \hat{\phi} \int_{-\infty}^{+\infty} d\omega \int_0^{+\infty} dk_{\perp} - i\omega \varepsilon_0 \varepsilon_{r1} A_1 2\pi J_1(k_{\perp}\rho) e^{-ik_{z1}z - i\omega t} \quad (S41)$$

$$\bar{H}_2^R(\bar{r}, t) = \hat{\phi} \int_{-\infty}^{+\infty} d\omega \int_0^{+\infty} dk_{\perp} - i\omega \varepsilon_0 \varepsilon_z 2\pi J_1(k_{\perp}\rho) (A_2^- e^{-ik_{z2}(z-d)} + A_2^+ e^{ik_{z2}z}) e^{-i\omega t} \quad (S42)$$

$$\bar{H}_3^R(\bar{r}, t) = \hat{\phi} \int_{-\infty}^{+\infty} d\omega \int_0^{+\infty} dk_{\perp} - i\omega \varepsilon_0 \varepsilon_{r3} A_3 2\pi J_1(k_{\perp}\rho) e^{ik_{z3}z - i\omega t} \quad (S43)$$

## S1.2 Angular spectral energy density of transition radiation

Moreover, we analytically calculate the angular spectrum of the transition radiation below. The angular spectral energy density can be expressed as

$$W = \int_0^{\frac{\pi}{2}} d\theta U(\theta) \cdot 2\pi \sin\theta \quad (S44)$$

where the radiation angle  $\theta$  corresponds to the angle made by the wavevector of emitted light  $\bar{k}$  and its component perpendicular to the interface  $\bar{k}_z$ .

The total radiated energy  $W$  into the vacuum regions can be obtained by integrating the emitted field energy density across all space as  $t \rightarrow \infty$ , since the emitted radiation field is separated from the charge field over a sufficiently long time. And for freely propagating waves, the electric and magnetic energy densities are equal in free space. Hence, the total radiated energy can be expressed as

$$W = \iint dx dy \int_{-\infty}^{+\infty} dz \varepsilon_{r1} |\bar{E}_1^R(\bar{r}, t)|^2 + \varepsilon_{r3} |\bar{E}_3^R(\bar{r}, t)|^2 \quad (S45)$$

$$|\bar{E}_1^R(\bar{r}, t)|^2 = \int d\omega d\omega' \iint d\bar{k}_{\perp} d\bar{k}'_{\perp} \bar{E}_{\bar{k}_{\perp}, \omega, 1}^R(z) \cdot [\bar{E}_{\bar{k}'_{\perp}, \omega', 1}^R(z)]^* e^{i[(\bar{k}_{\perp} - \bar{k}'_{\perp}) * \bar{r}_{\perp} - (\omega - \omega')t]} \quad (S46)$$

$$|\bar{E}_3^R(\bar{r}, t)|^2 = \int d\omega d\omega' \iint d\bar{k}_{\perp} d\bar{k}'_{\perp} \bar{E}_{\bar{k}_{\perp}, \omega, 3}^R(z) \cdot [\bar{E}_{\bar{k}'_{\perp}, \omega', 3}^R(z)]^* e^{i[(\bar{k}_{\perp} - \bar{k}'_{\perp}) * \bar{r}_{\perp} - (\omega - \omega')t]} \quad (S47)$$

By substituting equations (S46) and (S47) into (S45), we have

$$W = 2 \int_0^{+\infty} d\omega \int \varepsilon_{r1} |A_1|^2 \frac{\omega^2}{ck_{\perp}^2} \sqrt{\varepsilon_{r1} - \frac{c^2 k_{\perp}^2}{\omega^2}} (2\pi)^3 dk_{\perp} + \varepsilon_{r3} |A_3|^2 \frac{\omega^2}{ck_{\perp}^2} \sqrt{\varepsilon_{r3} - \frac{c^2 k_{\perp}^2}{\omega^2}} (2\pi)^3 dk_{\perp} \quad (S48)$$

Then, by comparing equation (S44) and (S48), the total angular spectral energy density of transition radiation can be written as

$$U(\theta) = (|A_1|^2 + |A_3|^2) \frac{16\pi^3 \omega^2 \varepsilon_0^{3/2} \mu_0^{1/2} \cos^2 \theta}{\sin^2 \theta} \quad (S49)$$

## Section S2. Photonic density of states of anisotropic epsilon-near-zero metamaterials

In this section, we analytically obtain the photonic density of states of anisotropic epsilon-near-zero metamaterials, namely the number of photonic eigenmodes per unit volume per frequency [89]. To begin with, the photonic density of states  $g(\omega)$  for isotropic materials can be expressed as  $g(\omega) = \frac{\varepsilon_r^{3/2} \omega^2}{2\pi^2 c^3}$ , where  $\varepsilon_r$  is the relative permittivity of isotropic materials. This expression corresponds to the volume of a shell in the momentum space bounded between two spherical surfaces, each defined by the frequencies  $\omega$  and  $\omega + d\omega$ , as illustrated in Figure S2a. Notably, not all eigenmodes in isotropic materials can couple into free space. For instance, in an isotropic material with the relative permittivity  $\varepsilon_r = 5$ , only the eigenmodes within the grey region of Figure S2a can safely couple into free space. Moreover, the eigenmodes in isotropic materials possess a trivial distribution in the  $k_\perp$  -  $k_z$  parameter space, which accounts for the poor directionality of transition radiation compared to anisotropic epsilon-near-zero metamaterials.

In contrast, anisotropic epsilon-near-zero metamaterials with the relative permittivity  $\bar{\varepsilon}_r = [\varepsilon_\perp, \varepsilon_\perp, \varepsilon_z]$  are featured with increased photonic density of states due to the elongated the spheroidal shape via  $\varepsilon_\perp \gg 1$ . To be specific, the anisotropic epsilon-near-zero metamaterials could accommodate more eigenmodes, and particularly, support the high-momentum eigenmodes, as shown in Figure S2b. On the other hand, the photonic eigenmodes tend to be confined in a narrow angular range, namely  $(0, \arcsin \sqrt{\varepsilon_z}]$ , due to  $\varepsilon_z \rightarrow 0^+$ .

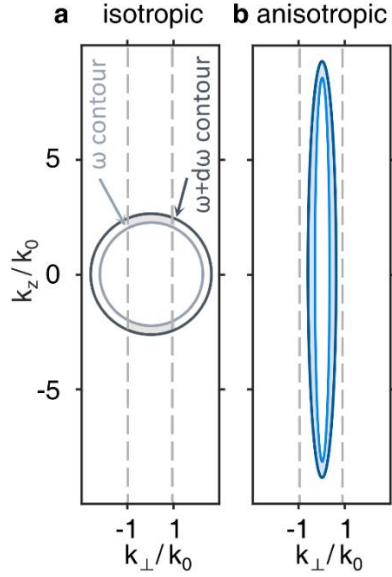


**Figure S2.** Conceptual demonstration for obtaining the photonic density of states of anisotropic metamaterial and isotropic material based on the isofrequency contour. (a) Isotropic material. (b) Anisotropic metamaterial. The grey and blue shaded regions.

### Section S3. More discussion of the Ultra-directional transition radiation from deep-subwavelength epsilon-near-zero metamaterials

S3.1 Possible experimental implementation of the epsilon-near-zero metamaterial required for the emergence of directional transition radiation

In this subsection, we show in Figures S3-S5 that the epsilon-near-zero metamaterial with the desired permittivity tensor (namely  $\epsilon_z \rightarrow 0$  and  $\epsilon_{\perp} \gg 1$ ) could be implemented and precisely tuned through an effective-medium approach [90].

Specifically, as shown in Figure S3a, the multilayer structure with effective parameters (e.g.  $h\text{BN}-\text{Bi}_2\text{Te}_3$  multilayer) is formed by alternately stacking the epsilon-near-zero material and high-index dielectric material. For example, as illustrated in Figure S3b-c, the precisely defined parameters of  $\epsilon_z = 0.1$  and  $\epsilon_{\perp} = 70$  used in the main text, could be achieved by tuning the filling ratios of the constituent  $h\text{BN}$  ( $\epsilon_z \rightarrow 0$ ) [91] and  $\text{Bi}_2\text{Te}_3$  ( $\epsilon_z = \epsilon_{\perp}$  reaching

100) [92]. Furthermore, we show in Figure S3d that the desired epsilon-near-zero metamaterial implemented by the multilayer structure could readily enables the emergence of directional transition radiation, even though the realistic material loss could degrade the radiation performance to some extent.

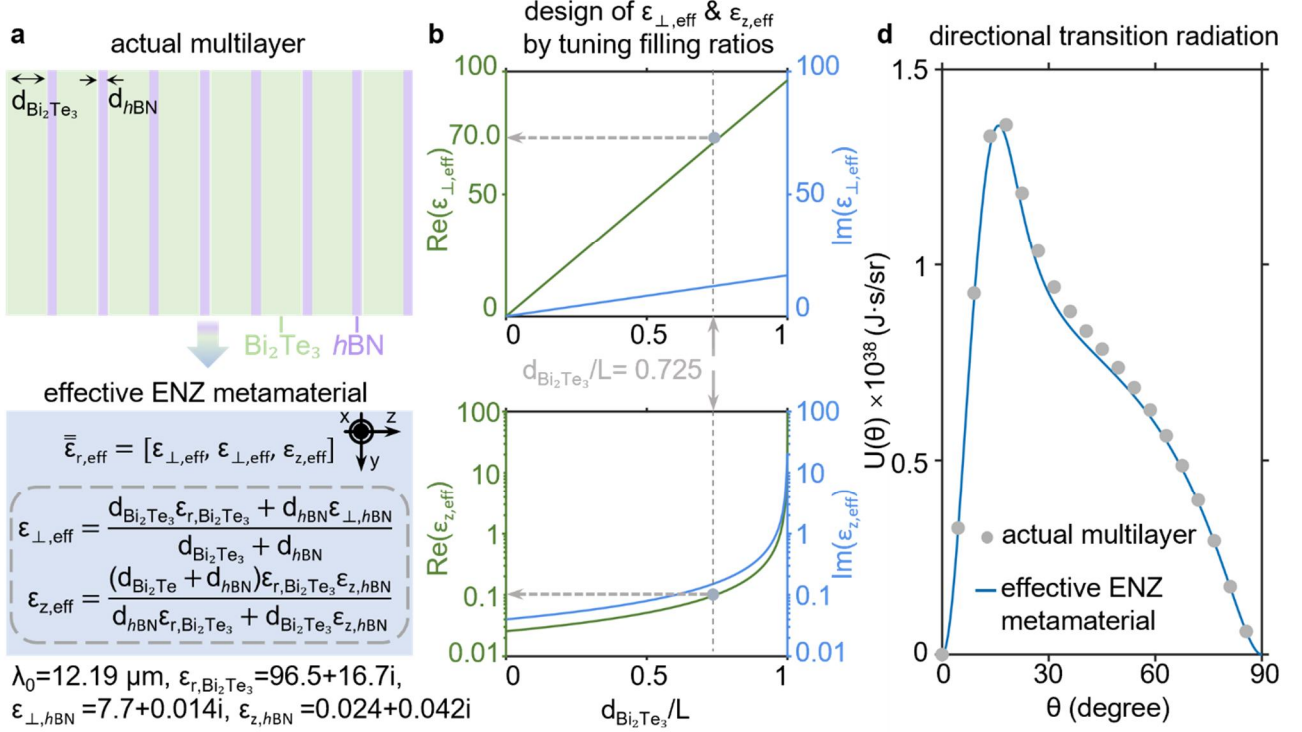


**Figure S3.** Experimental scheme for flexibly implementing the epsilon-near-zero metamaterial slab with desired parameters. For illustration here, the working wavelength  $\lambda_0 = 12.19 \mu\text{m}$ ,  $\epsilon_{z,\text{hBN}} = 0.024 + 0.042i$ ,  $\epsilon_{\perp,\text{hBN}} = 7.72 + 0.0135i$ , and  $\epsilon_{r,\text{Bi}_2\text{Te}_3} = 96.5 + 16.7i$  [91-92]. The multilayer has a total thickness of  $0.1 \lambda_0$  and consists of 50 unit cells. Within each unit cell,  $d_{\text{hBN}} = 6.70 \text{ nm}$  and  $d_{\text{Bi}_2\text{Te}_3} = 17.77 \text{ nm}$ . (a) Effective-medium approach to implementing the effective slab with effective parameters  $\epsilon_{z,\text{eff}} \rightarrow 0$  and  $\epsilon_{\perp,\text{eff}} \gg 1$ . (b,c) Precise design of the effective permittivity tensor by tuning the filling ratio of the constituents of the multilayer. (d) Angular spectral energy density of transition radiation from the actual multilayer and the effective slab. Directional transition radiation emerges from both actual and effective structures and agrees well with each other.

Furthermore, in Figure S4, we show in more detail that the effective medium approach allows us to achieve a considerably high effective out-of-plane permittivity of the  $\text{hBN}-\text{Bi}_2\text{Te}_3$  multilayer, e.g. equal to or larger than 70.

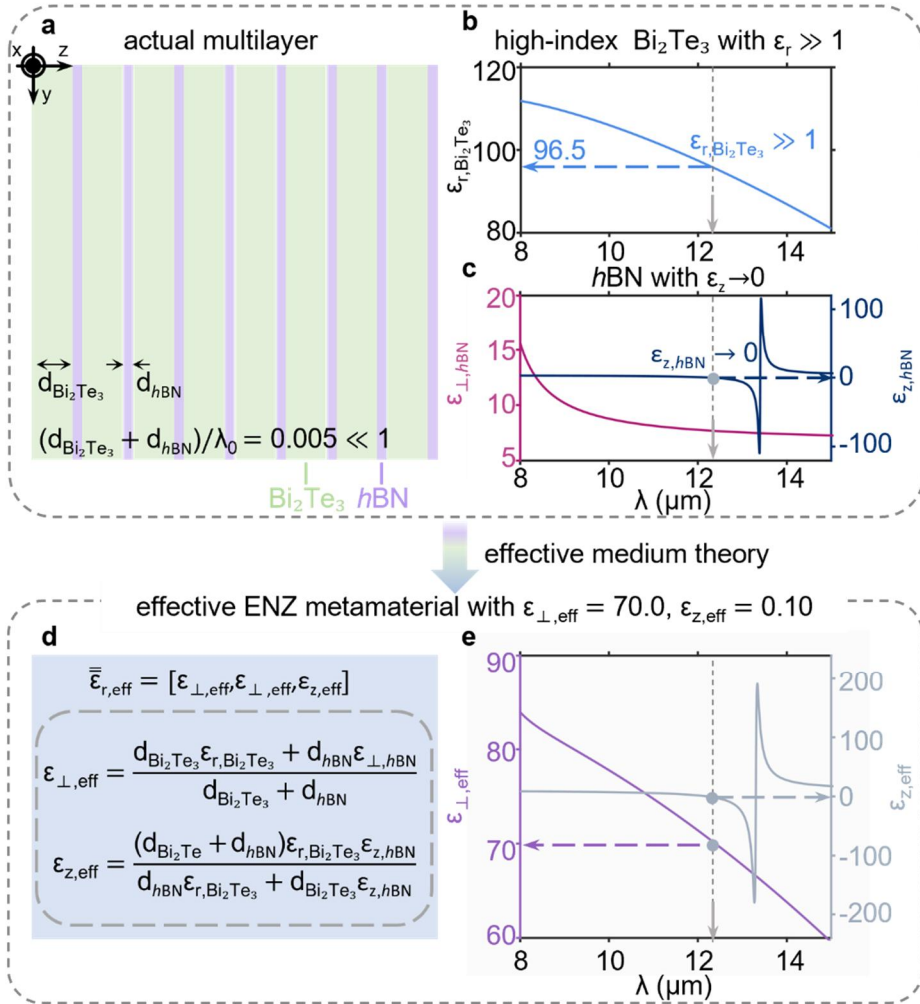


**Figure S4.** Effective-medium approach to manufacturing epsilon-near-zero metamaterial slab with large out-of-plane permittivity. (a) Multilayer structure formed by alternatively stacking high-index  $\text{Bi}_2\text{Te}_3$  and epsilon-near-zero  $h\text{BN}$ . For illustration here, the multilayer has a total thickness of  $0.1\lambda_0 = 1219 \text{ nm}$  and consists of 50 unit cells. Within each unit cell,  $d_{\text{Bi}_2\text{Te}_3} = 17.77 \text{ nm}$  and  $d_{h\text{BN}} = 6.70 \text{ nm}$ . (b,c) Real part of the permittivity of  $\text{Bi}_2\text{Te}_3$  [92] and  $h\text{BN}$  [91]. (d) Epsilon-near-zero metamaterial with effective permittivity tensor  $\bar{\epsilon}_{r,\text{eff}} = [\epsilon_{\perp,\text{eff}}, \epsilon_{\perp,\text{eff}}, \epsilon_{z,\text{eff}}]$  implemented by the effective medium theory. (e) Real part of the effective permittivity tensor. For example, when  $\lambda_0 = 12.19 \mu\text{m}$ , one has  $\epsilon_{z,\text{eff}} = 0.10$  and  $\epsilon_{\perp,\text{eff}} = 70.0 \gg 1$ .

Moreover, in Figure S5, we focus on the radiation performance of directional transition radiation emerging from the actual  $h\text{BN}-\text{Bi}_2\text{Te}_3$  multilayer and verify its agreement with the results from the epsilon-near-zero metamaterial slab with effective parameters.

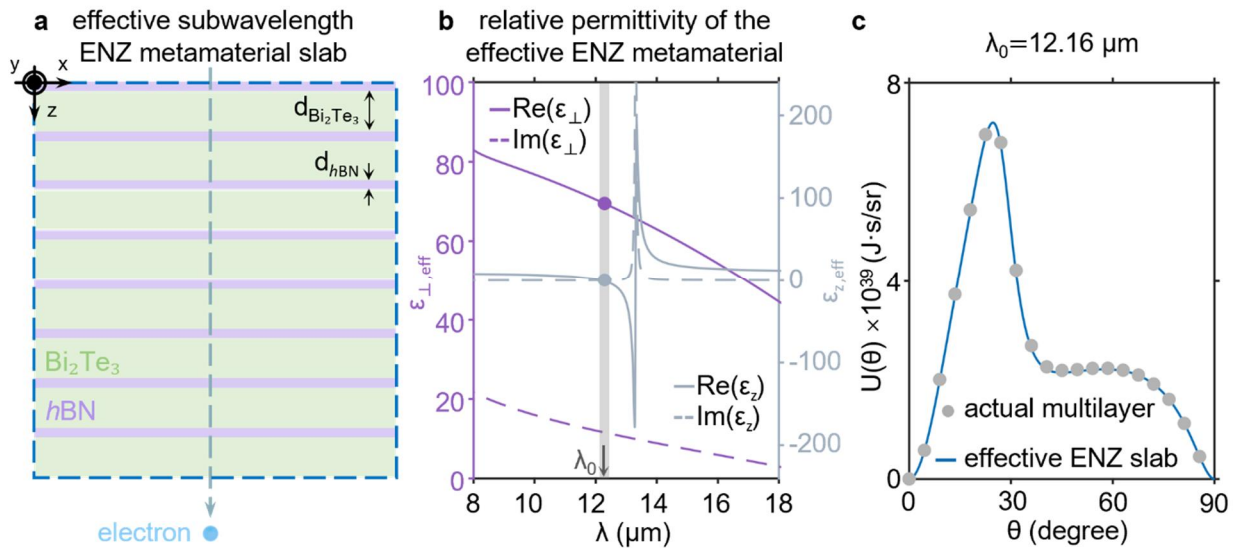


**Figure S5.** Ultra-directional transition radiation from an epsilon-near-zero metamaterial slab effectively implemented by realistic materials. (a) Structural schematic. A swift electron passes through a  $h\text{BN}-\text{Bi}_2\text{Te}_3$  multilayer. For illustration, the multilayer has a total thickness of  $0.1 \lambda_0 = 1216 \text{ nm}$  and consists of 50 unit cells. Within each unit cell,  $d_{h\text{BN}} = 6.68 \text{ nm}$  and  $d_{\text{Bi}_2\text{Te}_3} = 17.64 \text{ nm}$ . (b) Relative permittivity of the effective epsilon-near-zero metamaterial formed by the  $h\text{BN}-\text{Bi}_2\text{Te}_3$  multilayer. For example, at  $\lambda_0 = 12.16 \mu\text{m}$ , the effective parameters are  $\epsilon_{\perp,\text{eff}} = 70.0 + 12.2i$  and  $\epsilon_{z,\text{eff}} = 0.36 + 0.12i$ . (c) Angular spectral energy density of transition radiation from the actual multilayer and the effective epsilon-near-zero metamaterial slab. Notably, directional transition radiation emerges from the actual  $h\text{BN}-\text{Bi}_2\text{Te}_3$  multilayer and agrees well with the results for the epsilon-near-zero metamaterial slab with effective parameters.

### S3.2 Transition radiation from various types of epsilon-near-zero metamaterials

In this subsection, we show the radiation performance of transition radiation from various epsilon-near-zero metamaterials. In principle, our revealed ultra-directional transition radiation fundamentally requires the epsilon-

near-zero eigenmodes to concentrate at a certain emission angle (e.g. at the critical angle  $\theta = \theta_c$ ), which is in essence related to the eigen-wavevector component perpendicular to the electron's trajectory  $k_\perp$ , namely  $k_\perp = k_0 \sin \theta < k_0 \sqrt{\epsilon_z}$ . To this end, we show in Figure S6a the isofrequency contours of three types of anisotropic epsilon-near-zero metamaterials: type 1,  $\epsilon_z \rightarrow 0$  &  $\epsilon_\perp \gg 1$ ; type 2,  $\epsilon_z \rightarrow 0$  &  $\epsilon_\perp \rightarrow 0$ ; and type 3,  $\epsilon_z \gg 1$  &  $\epsilon_\perp \rightarrow 0$ . As further shown in Figure S6b, only the eigenmodes of type 1 of epsilon-near-zero metamaterials with  $\epsilon_z \rightarrow 0$  &  $\epsilon_\perp \gg 1$  are limited within a relatively narrow angular range. Consequently in Figure S6c, the ultra-directional transition radiation emerges only for epsilon-near-zero metamaterials with  $\epsilon_z \rightarrow 0$  and  $\epsilon_\perp \gg 1$ .

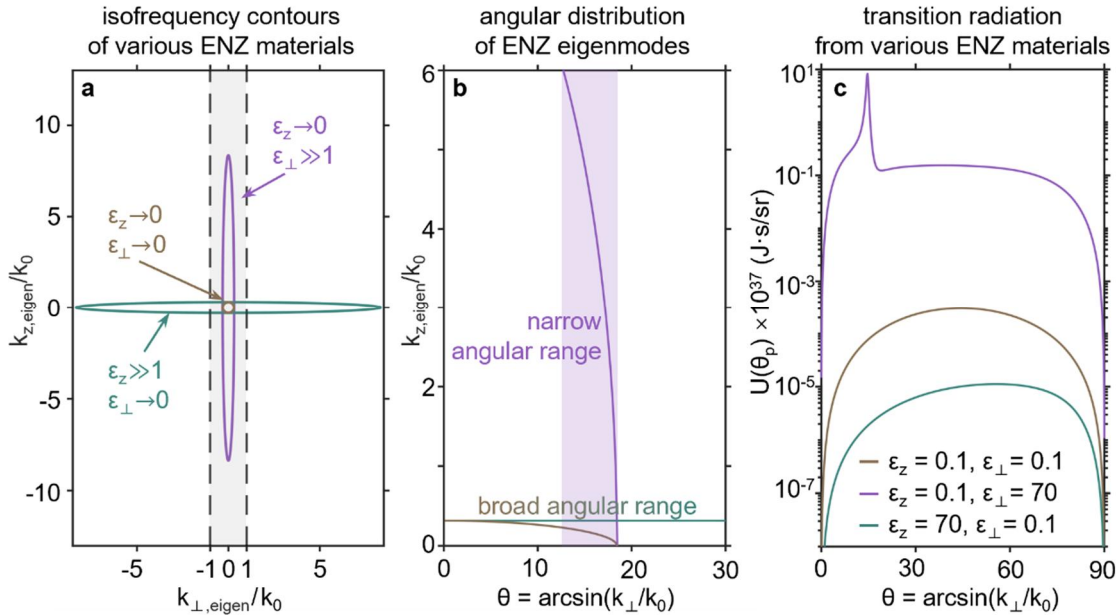


**Figure S6.** Transition radiation from various types of epsilon-near-zero metamaterials. (a,b) Isofrequency contours and angular distribution of eigenmodes inside various epsilon-near-zero metamaterials. (c) Angular spectral energy densities of transition radiation for these epsilon-near-zero metamaterials. Only epsilon-near-zero metamaterials with  $\epsilon_z \rightarrow 0$  and  $\epsilon_\perp \gg 1$  exhibit eigenmodes concentrated near a specific angle, thereby enabling ultra-directional transition radiation.

### S3.3 Influence of material loss on the performance of the ultra-directional transition radiation

In this subsection, we show the influence of material loss on the performance of ultra-directional transition

radiation from anisotropic epsilon-near-zero metamaterials with the relative permittivity  $\bar{\epsilon}_r = [\epsilon_{\perp}, \epsilon_{\perp}, \epsilon_z]$ . In fact, the revealed transition radiation has a certain degree of tolerance to the material loss from epsilon-near-zero metamaterials. For example, as shown in Figure S7, when the material loss is relatively small (e.g. loss tangent  $\tan \delta = \tan(\text{Im}(\epsilon)/\text{Re}(\epsilon)) \leq 30\%$ ), the transition radiation from epsilon-near-zero metamaterials could still emerge with a nearly one-order-of-magnitude enhancement in intensity and a relatively narrow angular spread less than ten degrees.

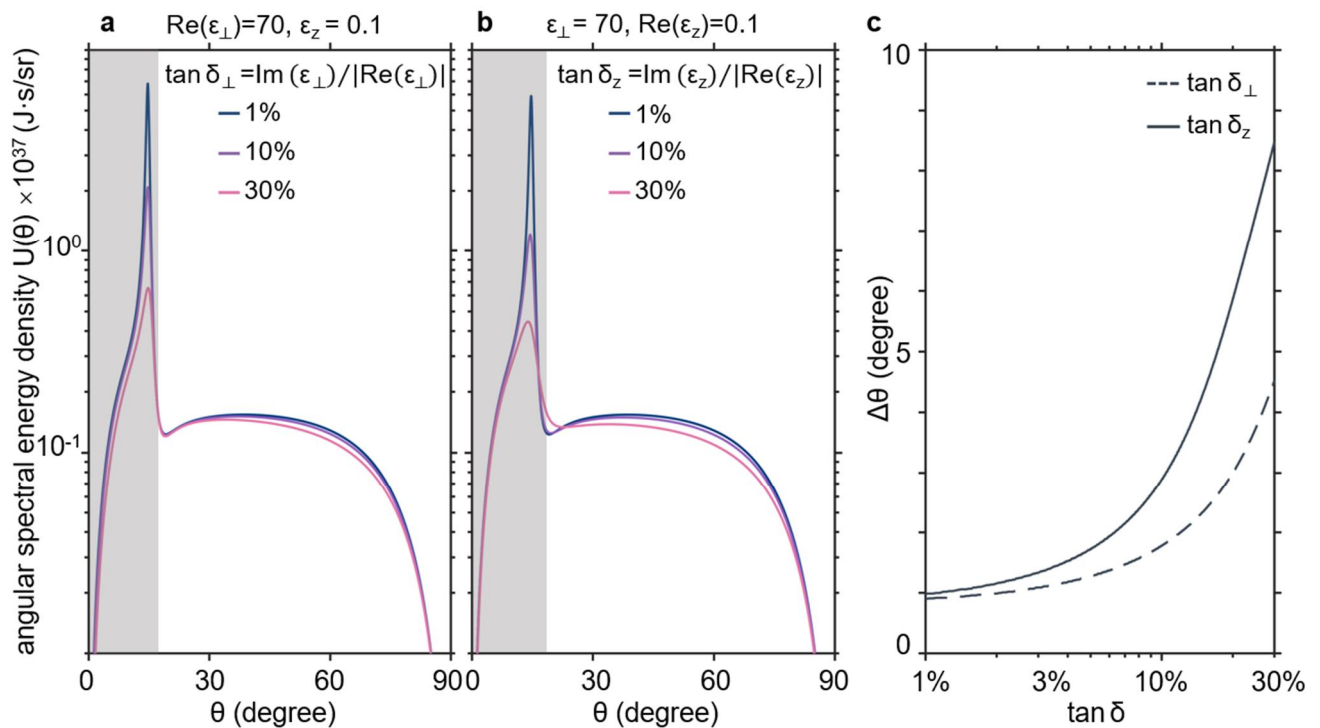


**Figure S7.** Influence of material loss on the performance of the ultra-directional transition radiation. The structural setup here is exactly the same as that in Figure 1 of the main text except that the material loss is introduced. (a,b) Dependence of the angular spectral energy density on the material loss. Material loss is added to  $\epsilon_{\perp}$  in (a) and  $\epsilon_z$  in (b). (c) Dependence of the angular width (i.e. angular full width at half maximum)  $\Delta\theta$  on the material loss. The enhanced intensity and characteristic directionality are persevered when the loss is relatively small, e.g. loss tangent  $\tan \delta = \tan(\text{Im}(\epsilon)/\text{Re}(\epsilon)) \leq 30\%$ .

### S3.4 Special phase variation of transition radiation inside the epsilon-near-zero metamaterial

In this subsection we investigate the special phase variation of transition radiation from epsilon-near-zero metamaterial. In epsilon-near-zero metamaterials, the phase of light could exhibit very small variations as it propagates, which is known as the light squeezing or tunnelling [93]. As shown in Figure S8a, our proposed epsilon-near-zero metamaterials with  $\epsilon_z \rightarrow 0$  make the eigen-wavevector component perpendicular to the electron's trajectory extremely small, namely  $|k_{\perp,\text{eigen}}|/k_0 < \sqrt{\epsilon_z} \rightarrow 0$ . Consequently, as illustrated in Figure S8b-c, the phase variation in that direction is negligible. Furthermore, as a supplement in Figure S8d, the plane-like phase front in the forward and backward vacuum regions verifies the emergence of directional transition radiation.

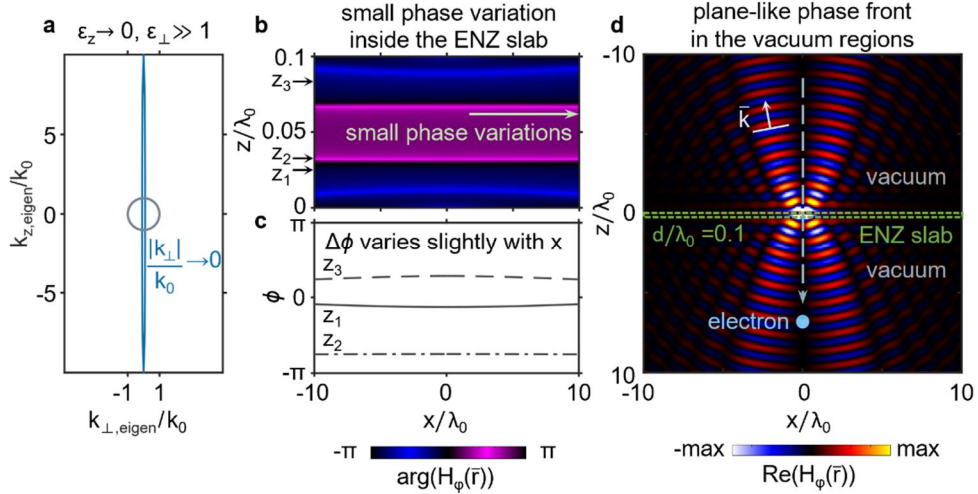


**Figure S8.** Special phase variation of transition radiation inside the epsilon-near-zero metamaterial. For illustration here,  $v/c = 0.1$ ,  $d/\lambda_0 = 0.1$ ,  $\epsilon_z = 10^{-4}$ , and  $\epsilon_{\perp} = 10^2$  (a) Isofrequency contours of the epsilon-near-zero metamaterials. (b) Phase of transition radiation  $\arg(H_{\phi}(\bar{r}))$  inside the epsilon-near-zero metamaterials. The phase is mapped in the  $x$  -  $z$  parameter space in (b) and shown at different vertical position  $z_1 = 0.03\lambda_0$ ,  $z_2 = 0.04\lambda_0$ , and  $z_3 = 0.085\lambda_0$  in (c). (d) Field distribution of the emitted directional transition radiation. Inside the metamaterial, the transition radiation exhibits extremely small phase variations in the  $\hat{x}$  direction due to  $\epsilon_z \rightarrow 0$ . In forward and backward vacuum regions, plane-like phase front indicates the emergence of directional transition radiation.

## Reference

- [89] C. Kittel, *Introduction to Solid State Physics* (Wiley, 1996).
- [90] J. Wu, Z. T. Xie, Y. Sha, H. Y. Fu, and Q. Li, Epsilon-near-zero photonics: infinite potentials. *Photonics Research* **9**, 1616, (2021).
- [91] J. D. Caldwell, I. Aharonovich, G. Cassabois, J. H. Edgar, B. Gil, and D. N. Basov, Photonics with hexagonal boron nitride. *Nature Reviews Materials* **4**, 552-567 (2019).
- [92] D. Singh, S. Nandi, Y. Fleger, S. Z. Cohen, and T. Lewi, Deep-subwavelength resonant meta-optics enabled by ultra-high index topological insulators. *Laser & Photonics Reviews* **17**, 2200841 (2023).
- [93] M. Silveirinha and N. Engheta, Tunneling of electromagnetic energy through subwavelength channels and bends using  $\epsilon$ -near-zero materials. *Physical Review Letters* **97**, 157403 (2006).